Nonviral Cell Labeling and Differentiation Agent for Induced Pluripotent Stem Cells Based on Mesoporous Silica Nanoparticles

Wei Chen,[†,⊥] Ping-Hsing Tsai,[‡,⊥] Yann Hung,[†] Shih-Hwa Chiou,[‡,§,*] and Chung-Yuan Mou[†,*]

[†]Department of Chemistry, National Taiwan University, Taipei 106, Taiwan, [‡]Institute of Pharmacology, National Yang-Ming University, Taipei 112, Taiwan, and [§]Department of Medical Research and Education, Taipei Veterans General Hospital, Taipei 112, Taiwan. [⊥]W. Chen and P.-H. Tsai contributed equally to this work.

ABSTRACT The generation of induced pluripotent stem cells (iPSCs) is an innovative personalized-regenerative technology, which can transform own-self somatic cells into embryonic stem (ES)-like cells, which have the potential to differentiate into all cell types of three dermal lineages. However, how to quickly, efficiently, and safely produce specific-lineage differentiation from pluripotent-state cells and iPSCs is still an open question. The objective of the present study was to develop a platform of a nonviral gene delivery system of mesoporous silica nanoparticles (MSNs) to rapidly generate iPSC-derived definitive-lineage cells, including endodermal-differentiated cells. We also evaluated the feasibility and efficiency of FITC-conjugated MSNs (FMSNs) for labeling of iPSCs and utilized the multifunctional properties of FMSNs for a suitable carrier for biomolecule delivery. We showed that FMSNs of various surface charges could be efficiently internalized by iPSCs without causing cytotoxicity. The levels of reactive oxygen species and pluripotent status, including *in vitro* stemness signatures and *in vivo* teratoma formation, remained unaltered. Notably, positive-charged FMSN enhanced cellular uptake efficiency and retention time. Moreover, when using positive-charged FMSN to deliver hepatocyte nuclear factor 3β (HNF3β) plasmid DNA (pDNA), the treated iPSCs exhibited significantly improved definitive endoderm formation and further quickly differentiated into hepatocyte-like cells with mature functions (low-density lipoprotein uptake and glycogen storage) within 2 weeks *in vitro*. Double delivery of pHNF3β further improved mRNA expression levels of liver-specific genes. These findings reveal the multiple advantages of FMSNs to serve as ideal vectors not only for stem cell labeling but also for safe gene delivery to promote the production of hepatocyte-like cells from iPSCs.

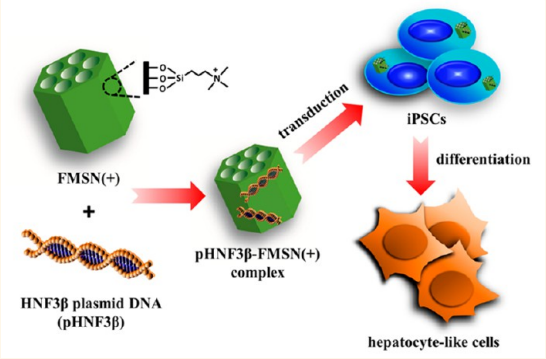

KEYWORDS: mesoporous silica nanoparticle · induced pluripotent stem cell · cell labeling · DNA delivery · hepatocyte-like cell

The development of induced pluripotent stem cells (iPSCs) has opened a new era for stem cell research. Ectopic expression of four key transcription factors (Oct4, Sox2, Klf4, and c-Myc) directly reprograms somatic cells into pluripotent cells, which exhibit similar characteristics to embryonic stem (ES) cells[1,2] without ethical issues. In addition, iPSCs could overcome immunological rejection since autologous patient-specific iPSCs can be easily derived. The generation of patient- or disease-specific iPSCs therefore holds promising potential for the drug industry and regenerative medicine.[3] Despite the great potential of iPSC technology,[4−7] there are many hurdles and challenges to be solved before applying iPSCs in clinical treatment. To comprehensively elucidate the potential of iPSCs for therapeutic application, appropriate labeling and tracking of iPSCs should be established.

Liver failure can result from acute insults or chronic persistent damages, and the curative management of liver failure is orthotopic liver transplantation.[8,9] Unfortunately, liver transplantation has several major limitations, such as donor organ shortage and high cost.[10] The generation of iPSCs transforms own-self somatic cells into ES-like cells and holds the potential to differentiate into all cell lineages, including hepatocytes.[11] Notably, an effective platform for hepatocyte generation from patient-specific iPSCs was reported to model inherited metabolic liver

* Address correspondence to cymou@ntu.edu.tw; shchiou@vghtpe.gov.tw.

Received for review March 21, 2013 and accepted September 24, 2013.

Published online September 24, 2013
10.1021/nn401418n

disorders.[12] In addition, senescent and centenarian-derived iPSCs are able to redifferentiate into fully rejuvenated cells.[13] However, several hurdles exist in iPSC reprogramming and its practical application. To control the fate of differentiation, growth factors in the culture medium are routinely used; however, growth factor-based induction often requires a long period for specific-lineage induction, especially in hepatic differentiation.[14] Even efficient generation of functional hepatocytes by gene transduction of a viral-based system has recently been reported;[15,16] the use of viral vectors remains risky and is unfavorable for clinical treatment.

In the past decade, mesoporous silica nanoparticles (MSNs) have attracted much attention for their preeminent attributes including high surface area (about 1000 m^2/g), adjustable pore size (2−20 nm), and easy functionalization. This could be a versatile platform for diagnosis and therapeutics through incorporation of multifunctional materials.[17] MSNs can simultaneously possess fluorescence[18,19] and magnetic properties and can act as carriers for drugs and biomolecules.[20−28] These excellent intrinsic properties have been broadly demonstrated in biomedical applications.[17,29−37] In addition, MSNs exert remarkably little cytotoxicity and have no adverse effect on various cell types both *in vitro* and *in vivo*.[17,38,39] This biocompatibility makes them superior multifunctional nanomaterials for biomedical niche applications.

The integration of nanomaterials and biology has influenced modern nanomedicine, especially toward personalized medicine.[40] We previously reported that 100 nm FITC-conjugated MSNs (FMSNs) can efficiently enter 3T3-L1 cells and human mesenchymal stem cells.[41] Ruan *et al*. used Generation 5.0 polyamidoamine dendrimer-modified magnetic nanoparticles as a delivery system to package four transcription factors, *i.e*., Nanog, Sox2, Lin28, and Oct4, into 293T cells.[42] Moreover, Cho's group used magnetic nanoparticles as a transfection platform to generate iPSCs efficiently.[43] However, up to now, a gap appears to exist between nanotechnology and iPSCs. The interactions between iPSCs and nanoparticles have not been reported yet. More specifically, the application of MSNs has never been exploited in iPSCs.

In this study, we explored the applications of FMSNs in iPSCs. Three different types of fluorescent MSNs were examined, namely, unmodified FMSN (FMSN(u)), positively charged FMSN (FMSN(+)), and negatively charged FMSN (FMSN(−)). We investigated the uptake of the nanoparticles by the iPSCs and the response of iPSCs to the nanoparticles. We found that, like other mammalian cells albeit smaller (iPSCs are slightly larger than 10 μm), iPSCs would take up FMSNs efficiently. By manipulating the surface charge of the nanoparticles, we demonstrated that positively charged FMSN(+) were more efficiently internalized by the iPSCs. All three types of nanoparticles entered without impairing cell viability and pluripotent capability, including *in vivo* teratoma formation with tridermal-lineage differentiation. Then we explored the FMSN(+) as a delivery vehicle for the iPSCs. For FMSN(+) carrying hepatocyte nuclear factor 3β (HNF3β) plasmid DNA (pDNA), we established an efficient nonviral gene-delivery system to improve definitive hepatic induction. We developed a platform that is able to shorten the differentiation period and generate functional hepatocyte-like cells from iPSCs (Scheme 1). This may offer an alternative approach for translational therapeutics, especially in the treatment of liver diseases. Our results not only demonstrated the potential for stem cell labeling but also revealed that FMSNs can act as a carrier for iPSCs delivering genes to the cells.

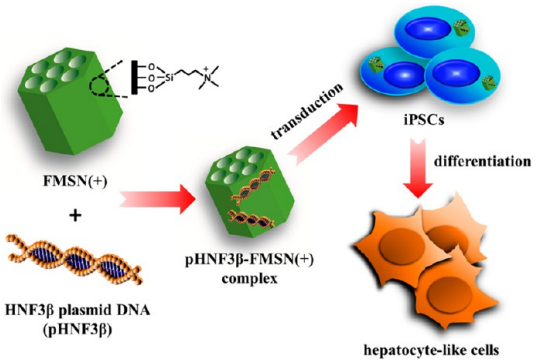

Scheme 1. HNF3β plasmid DNA (pHNF3β) was adsorbed on the positive-charged FMSN (FMSN(+)) to form a pHNF3β-FMSN(+) complex, which was internalized by iPSCs. The treated iPSCs exhibited significantly improved definitive endoderm formation and further quickly differentiated into hepatocyte-like cells with mature functions (low-density-lipoprotein uptake and glycogen storage) within 2 weeks *in vitro*.

RESULTS AND DISCUSSION

Characterization of FMSNs. Fluorescent FMSNs were synthesized using the method in our previous reports,[18,41] which was based on a sol−gel synthetic strategy in the presence of cationic surfactant templates. To investigate the charge effect on the cellular uptake, FMSN(u) was grafted with *N*-trimethoxysilylpropyl-*N*,*N*,*N*-trimethylammonium chloride (TA) and sodium 3-trihydroxysilylpropylmethylphosphonate (THPMP) to produce positively and negatively charged nanoparticles, respectively.[44] Transmission electron microscope (TEM) images of these FMSNs (Figure 1a) exhibited well-ordered hexagonal mesopores even after TA (Figure 1b) and THPMP (Figure 1c) modifications. The average sizes of FMSNs were around 110 nm (Supporting Information, SI, Figure S1a−c). Small-angle X-ray diffraction patterns, 2θ = 2.2°, 3.8°, and 4.4°, also supported the well-ordered 2D hexagonal arrangements (Figure 1d). N_2 adsorption/desorption isotherms of different FMSNs were measured at 77 K (SI, Figure S2a). Data on the textural characteristics are summarized

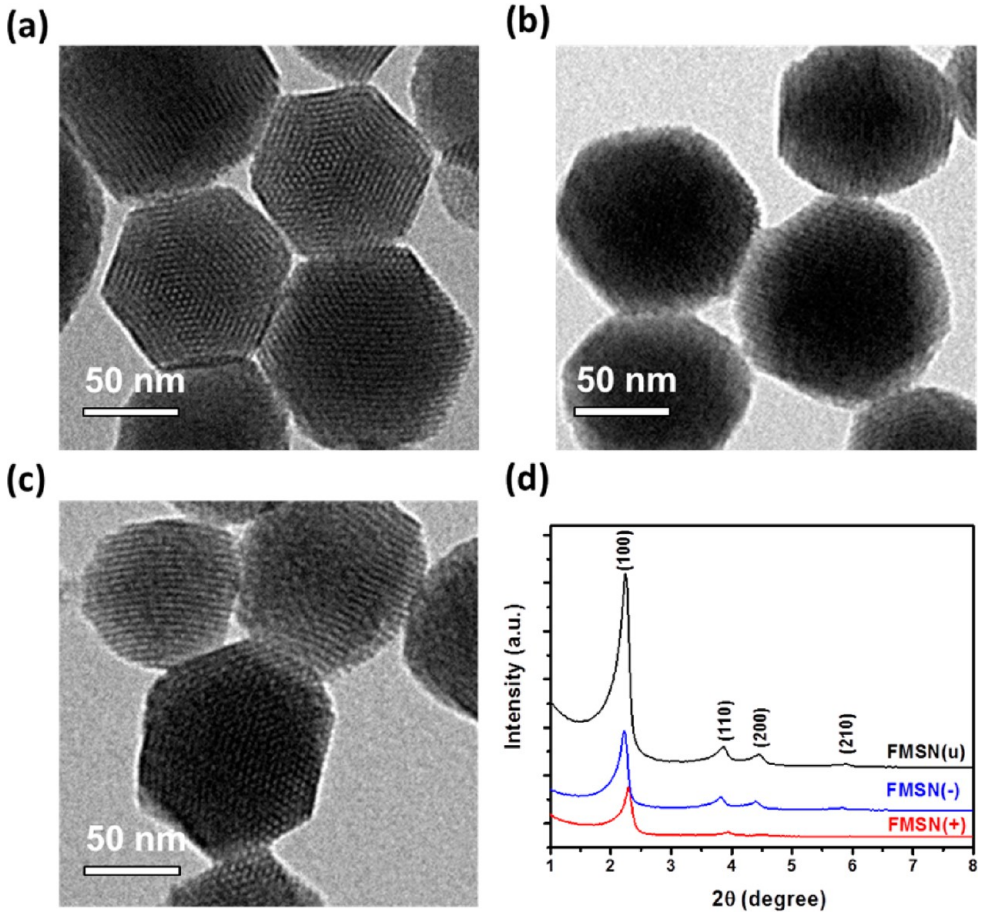

Figure 1. TEM images of (a) FMSN(u), (b) FMSN(+), and (c) FMSN(−). (d) Small-angle X-ray diffraction patterns of different FMSNs. The (100), (110), (200), and (210) diffraction peaks are characteristic 2D hexagonal structure.

in Table S1. The high surface area is a characteristic property of the mesostructured FMSNs; this provides an advantage to FMSNs as a platform to study iPSCs.

The FMSNs dispersed well in either water or Dulbecco's modified Eagle medium (DMEM). The average dynamic light scattering (DLS) size of FMSNs in H_2O was about 150 nm, similar to that in DMEM (SI, Figure S2b,c). pH-dependent zeta potentials of FMSNs confirmed the modification with THPMP and TA (SI, Figure S2d). Because of the quaternary ammonium groups on the surface of FMSN(+), its zeta potential in water (pH = 7.4) was +26 mV, much more positive than that of FMSN(u) (−15 mV) and THPMP-modified FMSN(−) (−45 mV). This design strategy can easily adjust the surface property of FMSNs in investigating the cells' uptake phenomenon. In addition, fluorescence spectra (SI, Figure S2e) of FMSNs confirmed that FITC was successfully conjugated in the framework of MSNs. Fluorescence spectra of the nanoparticles show the typical emission profiles of FITC and display similar intensities for the three types of FMSNs. Furthermore, the fluorescent intensity also remained the same after 42 h, indicating the dye was stable and remained on the FMSNs (SI, Figure S3).

FMSNs Are Internalized by iPSCs. *Time- and Dosage-Dependent Uptake by iPSCs.* A fundamental study of the interactions between nanoparticles and iPSCs was performed to examine the cellular uptake of FMSNs. iPSCs were incubated in the DMEM with FMSNs at various concentrations (25, 50, and 85 μg/mL) for different periods (0.5, 1, 2, and 4 h). Trypan blue was used to quench the fluorescence from the FMSNs adsorbed onto the outside of the cell.[45] Because trypan blue does not enter cells, it quenches the fluorescence of nanoparticles only on the outer cell membrane, but not those inside the cells.[46] Thus, the fluorescence we detected was only from the nanoparticles inside the cells. Through this quenching method, our data reflected the uptake of the nanoparticles. Intracellular fluorescence in live cells was then determined by flow cytometry analysis (Figure S4−S6) to quantify the cellular uptake of the nanoparticles. Time- and dosage-dependent uptake by iPSCs was observed for all three FMSNs (Figure 2a−c). We found uptake of FMSNs began as early as 0.5 h after the incubation. The mean fluorescence intensity (MFI) statistics of the iPSCs after incubation also demonstrated the time and dosage dependence. When the incubation dosage was increased to 100 μg/mL for 4 h (Figure 2d), more uptake

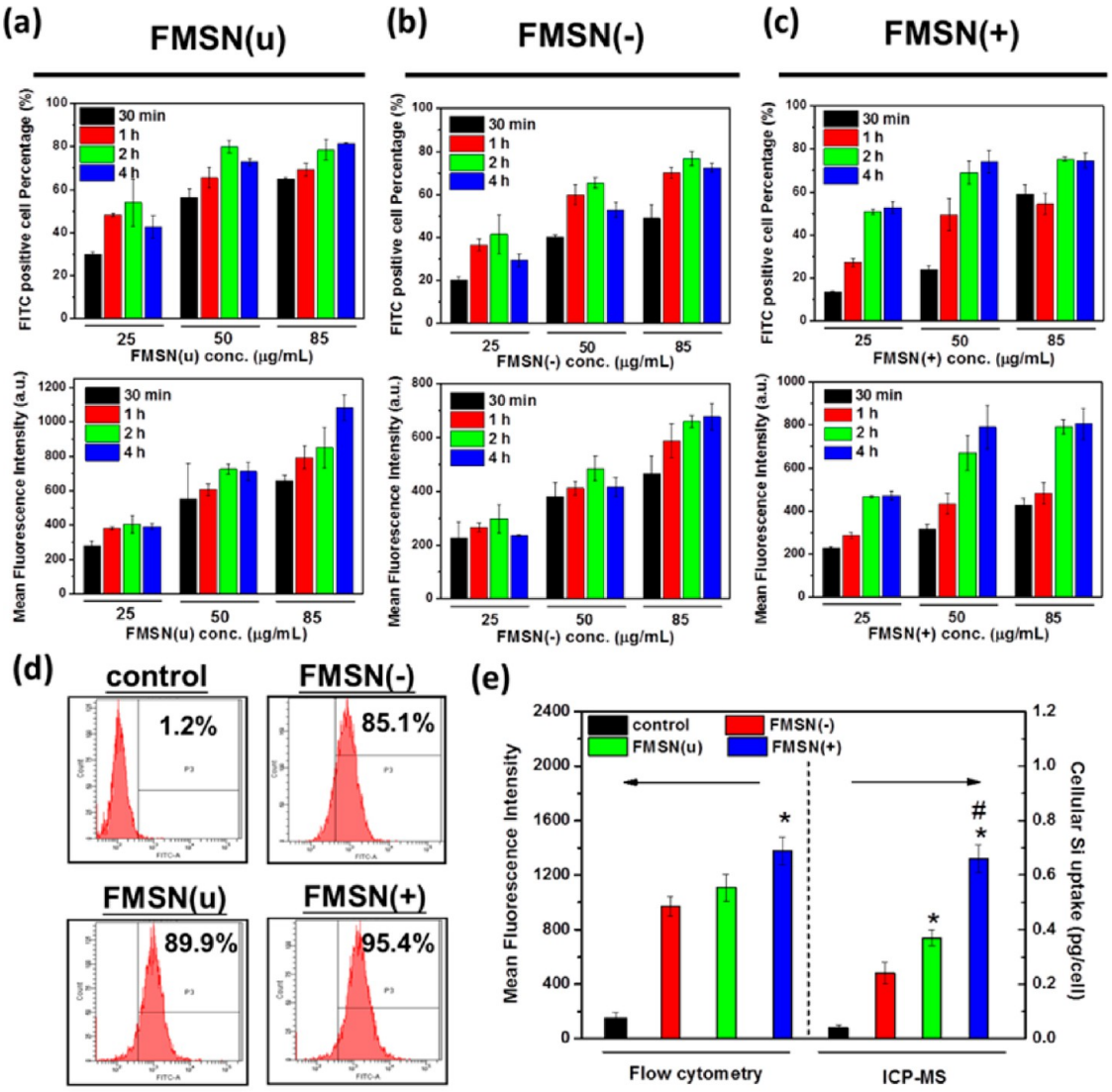

Figure 2. Time- (0.5, 1, 2, and 4 h) and dosage-dependent (25, 50, and 85 μg/mL) flow cytometry analyses of iPSCs after incubation with (a) FMSN(u), (b) FMSN(−), and (c) FMSN(+). The percentage of positively labeled cells and MFI of iPSCs were quantified and presented in the upper and lower panels, respectively. Data are presented as means ± SD of three independent experiments. (d) Representative flow cytometry histograms of iPSCs after incubation with FMSNs (100 μg/mL, 4 h). Control is incubation with no nanoparticles. (e) MFI of iPSCs and silicon uptake per iPSCs post FMSN incubation (100 μg/mL, 4 h). Data are presented as means ± SD of three independent experiments. Asterisks indicate statistically significant difference ($p < 0.05$) as compared with FMSN(−), and the pound sign indicates statistically significant difference ($p < 0.05$) as compared with FMSN(u).

was observed for all the FMSNs (approximately 90%). In addition, iPSCs after incubation with FMSN(+) gave substantially higher MFI, showing a statistical difference from FMSN(−) (Figure 2e). Confocal laser scanning microscope (CLSM) images also verified the cellular internalization of all FMSNs. This provides a notable advantage for FMSNs as labeling probes for the iPSCs and their further usage as carriers.

To further determine the quantity of FMSNs internalized, ICP-MS was used. After 4 h incubation with FMSNs at 100 μg/mL, the amount of silicon in the iPSCs was determined (Figure 2e). Results showed that the mass of silicon per cell was correlated to the zeta potential of FMSNs, and the cellular uptake was in the order FMSN(+) > FMSN(u) > FMSN(−), which agrees with the results of flow cytometry measurements. Among all the FMSNs tested, the one carrying positive charge, FMSN(+), resulted in the highest fluorescent intensity. This suggests that the surface charge of FMSNs affects the cellular uptake of iPSCs, agreeing with previous reports on 3T3-L1, mesenchymal stem cells, and neural stem cells.[18,47]

Mechanism of FMSN Uptake and Intracellular Distribution. Various inhibitors were used to explore the cell uptake mechanism. Cells were pretreated with the inhibitors, and the uptake was determined by flow cytometry analysis (Figures 3 and S7). The results indicate that fewer nanoparticles were internalized as

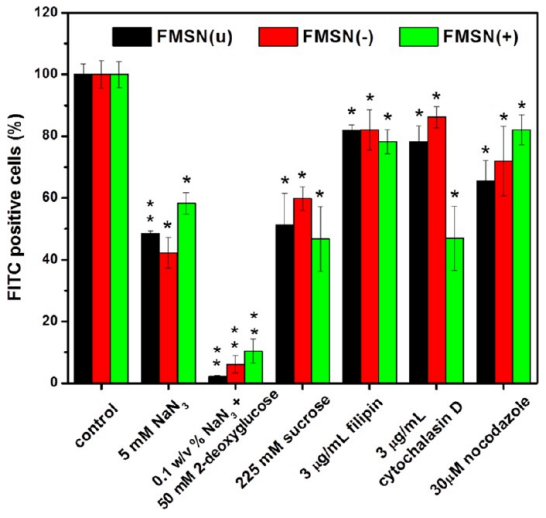

Figure 3. Flow cytometry examinations of the effect of pharmaceutical inhibitors on the cellular uptake of FMSNs. Inhibitor-pretreated iPSCs after co-incubation with FMSNs (100 μg/mL, 4 h) were analyzed. The controls were defined as those without inhibitor pretreatments. Data are means $\pm$ SD of three independent experiments. Asterisks and double asterisks indicate statistical differences (p < 0.05 and 0.01) compared with the respective control.

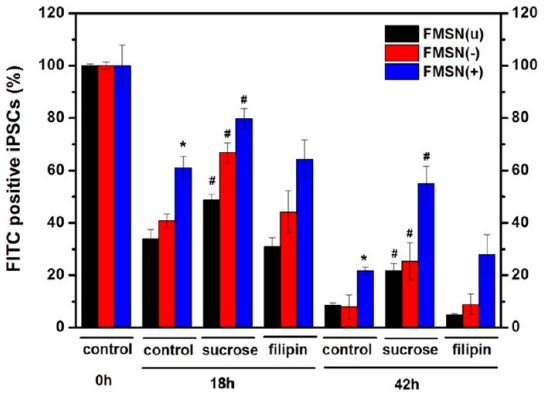

Figure 4. Flow cytometry evaluation of the FITC-positive iPSCs after 4 h FMSN incubation and regrowth in the regular medium with or without inhibitors (113 mM sucrose or 3 μg/mL filipin) for 0, 18, and 42 h. Data are means $\pm$ SD of three independent experiments. Asterisks indicate statistical differences (p < 0.05) compared with FMSN(u) and FMSN(−). Pound signs indicate statistically significant differences (p < 0.05) compared with respective time control.

more ATP was depleted by a mixture of sodium azide and 2-deoxyglucose;[48,49] almost 90% of the iPSC uptake was blocked by the inhibitors. Therefore, uptake of the nanoparticles is through an energy-dependent endocytosis. In addition, in the presence of sucrose, an inhibitor for clathrin-mediated endocytosis,[50,51] about 50% of the cell uptake was blocked, while only about 20% was inhibited by the presence of filipin, an inhibitor for caveolae-mediated endocytosis.[52,53] This implies that the majority of the nanoparticles enter by clathrin-mediated endocytosis. Therefore, like other cells, the iPSCs take up the FMSNs by clathrin-mediated endocytosis.[18,19] It appears that microfilaments control the FMSN(+) uptake because about 50% of the uptake was inhibited in the presence of cytochalasin D, an inhibitor for actin polymerization.[54,55] Moreover, the effect of nocodazole, an inhibitor for microtubule formation,[56] was also examined. Results suggest that both microtubules and microfilaments were involved in the uptake of FMSN(u) and FMSN(−).

Once FMSNs enter iPSCs by an endocytic pathway, they are entrapped inside early endosomes first and then transported to late endosomes−lysosomes. During this process, the nanoparticles could be released to the cytosol. To assess the intracellular distributions of the nanoparticles, co-localization experiments were carried out. FM4-64 dye is commonly used to study endocytosis, vesicle trafficking, and organelle organization in living eukaryotic cells.[57] After FMSN uptake, iPSCs were cultured with FM4-64. As shown in the confocal microscopic results (Figure S8), a punctate cytoplasmic distribution pattern for all FMSNs was observed. Some FMSNs (green) co-localized with FM4-64 (red, the marker of endosomes) as detected by yellow spots, but some did not. This suggests that some nanoparticles had been released to the cytoplasm.

Retention Time and Exocytosis of FMSNs in the iPSCs. To track stem cells, we evaluate the retention time of the fluorescent probes inside the iPSCs. Accordingly, after the 4 h incubation of FMSNs, iPSCs were washed, harvested, and recultured in DMEM. At predetermined times, the green fluorescence of the FMSNs remaining in the iPSCs was quantified by flow cytometry (Figure S9). Figure 4 displays the FITC-positive iPSCs (controls in the figure) *versus* the time postuptake of FMSNs. After 18 h regrowth, the percentage of FITC-positive iPSCs declined to about 35%, 40%, and 60% for FMSN(u), FMSN(−), and FMSN(+), respectively. After 42 h, the FITC-positive iPSCs further decreased to less than 10% for FMSN(u) and FMSN(−), compared to about 20% for FMSN(+). Hence, the percentages of FITC-positive iPSCs steadily decreased as time went on, probably due to the general cell division (doubling time ~18h)[1] and exocytosis. However, FMSN(+) appears to be retained slightly longer than the other two types of FMSNs. Ready exocytosis of MSN has been reported in human umbilical vein endothelial cells[58] and many other cells.[59]

We therefore carried out exocytosis studies. After the 4 h FMSN treatment, the iPSCs were incubated with or without inhibitors[60−62] (113 mM sucrose or 3 μg/mL filipin) for 18 and 42 h. The green fluorescence of the FMSNs remaining in the iPSCs was quantified by flow cytometry (Figure S9). In the presence of sucrose, the FITC-positive iPSCs were roughly 20% more than the respective control (without inhibitors) after 18 or 42 h incubation (Figure 4). Moreover, filipin did not affect the percent FITC-positive cells. Therefore, the decline of FITC-positive iPSCs could be attributed to exocytosis and general cell division (doubling time is about 18 h).

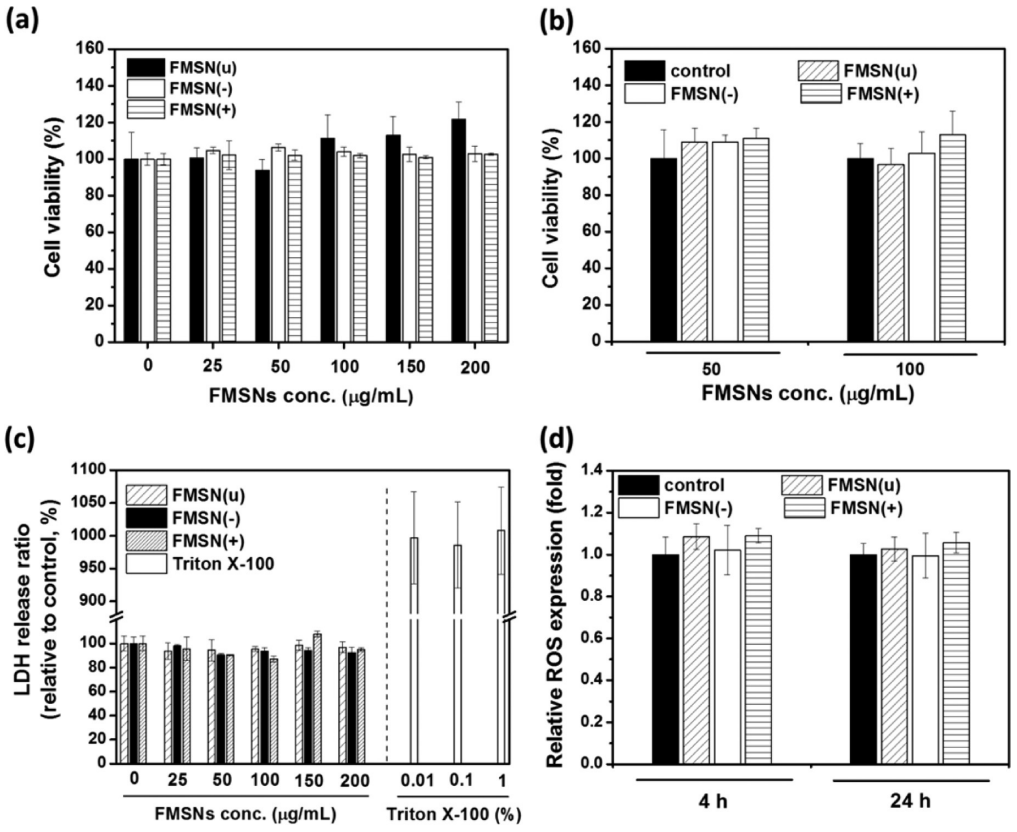

Figure 5. (a) Cytotoxicity of different FMSNs. iPSCs were incubated with different FMSNs at various concentrations for 4 h, and the viability was determined by a WST-1 assay. Data are means ± SD of six independent experiments. (b) Effect of different FMSNs on cell proliferation evaluated by a WST-1 assay. After cells were incubated with different FMSNs for 4 h, cells were allowed for growth in regular medium for 40 h. Data are means ± SD of six independent experiments. (c) Normalized LDH release from iPSCs after 4 h incubation with different FMSNs. Data are means ± SD of six independent experiments. (d) ROS levels among control (no nanoparticle treatment) and FMSN(u)-, FMSN(−)-, and FMSN(+)-treated iPSCs. Four hours (or 24 h) after FMSN uptake, the intracellular ROS level of iPSCs was detected by dihydroethidium and quantified by flow cytometry. Data are means ± SD of three independent experiments.

Cytotoxicity of FMSNs on iPSCs and Reactive Oxygen Species (ROS) Level. Cell viability and proliferation are cytotoxicity markers. A colorimetric WST-1 assay was used to assess the cell viability and proliferation. The cell viabilities of iPSCs after 4 and 24 h incubation with selected concentrations of FMSNs are shown in Figure 5a and Figure S10, respectively. No significant viability decrease was detected even at a very high concentration (200 μg/mL). In addition, the iPSC proliferation (Figure 5b) was not hindered in a 40 h growth in DMEM supplemented with 10% fetal bovine serum (FBS) post FMSN treatments. Furthermore, a lactate dehydrogenase (LDH) assay was also employed to evaluate if there was loss of membrane integrity resulting from either apoptosis or necrosis. Figure 5c displays the LDH release relative to control *versus* concentration of FMSNs. None of the FMSN-treated cells showed apparent LDH release after the 4 h incubation; that is, no severe membrane disruption was observed. A cell membrane disruption positive control was also performed by incubating with the nonionic surfactant Triton X-100. On the contrary, a considerable amount (around 1000%) of LDH was released and detected. Therefore, the FMSNs have little cytotoxicity and are suitable for cellular labeling.

A more in-depth examination of the cytotoxicity of the nanoparticles was performed to determine the intracellular ROS production, which indicates whether the cells are under oxidative stress. After incubating with FMSNs for 4 h, the intracellular ROS level was detected by a ROS dye, dihydroethidium, DHE. DHE is oxidized to the highly reddish fluorescent dye 2-hydroxyethidium in the presence of ROS, especially superoxide anions.[63] Flow cytometry results showed that neither FMSN(u), FMSN(−), nor FMSN(+) exerted a considerable effect on the ROS level for iPSCs at 4 h (Figure 5d). After further growth for 24 h in DMEM, intracellular ROS levels of all FMSN-treated iPSCs displayed no significant difference from the control. This low ROS stress is significant for FMSN application considerations.

FMSNs Do Not Disturb the Pluripotency of iPSCs. Self-renewal and pluripotency are the central features in the definition of ES cells as well as iPSCs, and Oct4 (octamer-binding transcription factor 4) is a key factor in this process.[64] Oct4 is a member of the POU-domain

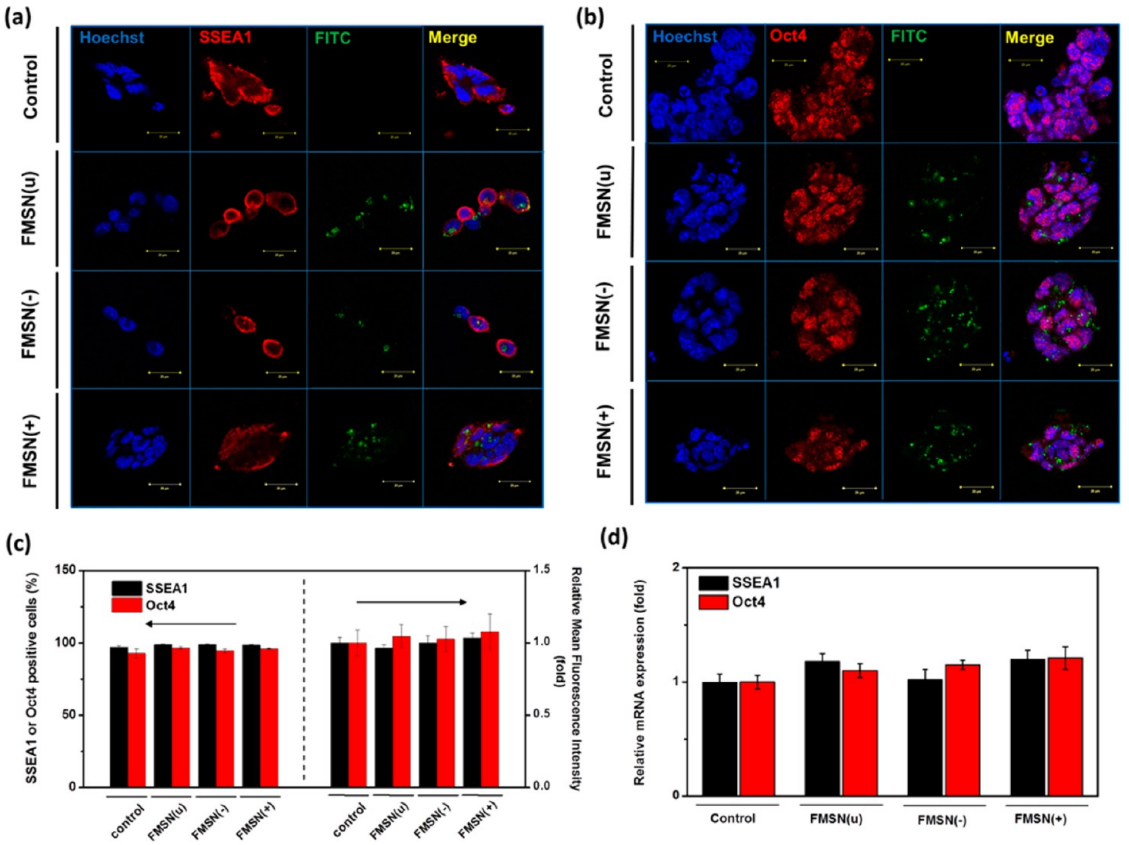

Figure 6. Immunofluorescence staining confocal microscope images of iPSCs after 4 h incubation with different FMSNs at a dosage of 100 μg/mL (control = no FMSNs). (a) Panels from left are the nucleus of iPSCs counterstained by Hoechst 33342, iPSC-specific surface marker SSEA1, FMSNs, and the merged images. (b) Panels from left are the nucleus of iPSCs counterstained by Hoechst 33342, anti-Oct4 antibody, FMSNs, and the merged images. Scale bars are 20 μm. (c) Flow cytometry analysis and quantification of iPSC stemness markers (SSEA1 and Oct4) after incubation with different FMSNs (100 μg/mL, 4 h). (d) Relative mRNA levels of the stemness markers (SSEA1 and Oct4) of iPSCs after incubation with different FMSNs (100 μg/mL, 4 h).

family of transcription factors and is expressed in the blastocyst, pluripotent embryonic stem, and germ cells.[64−66] Expression of Oct4 is down-regulated during differentiation, indicating that Oct4 plays a critical role in mammalian tissue development.[67] A primary consideration is whether the presence of nanoparticles would affect the pluripotency of the stem cells. To address this question, Oct4 and stage-specific embryonic antigen 1 (SSEA1, a surface marker of mouse ES cells and iPSCs)[68] were examined by the immunofluorescent staining of cells after FMSN internalization. First, as shown in the CLSM images in Figure 6a, the punctate cytoplasmic distribution of green fluorescence derived from FMSNs was inside the cell whose surface marker, SSEA1, was stained with red fluorescent anti-mouse SSEA1 DyLight 594 conjugate. The maintenance of SSEA1 in iPSCs implies that iPSCs remain in the undifferentiated state after incubation with FMSNs. In Figure 6b, our data revealed the CLSM images of iPSCs after FMSN treatment and stained with anti-mouse Oct4 DyLight 594 conjugate. Expression of the pluripotent marker Oct4 (red) was easily observed inside the nucleus of the cells (blue), whereas green fluorescence of FMSNs was distributed peripherally around the nucleus. These findings also agree with the above SSEA1 observation, that iPSCs were undifferentiated and their characteristic markers were preserved. CLSM images explicitly provide evidence that FMSNs are internalized without interfering with the expression of iPSC markers.

To further quantitatively determine the expression levels of stemness signature in FMSN-treated iPSCs, flow cytometry was used to quantify the Oct4- and SSEA1-positive iPSCs after the 4 h incubation and immunofluorescent staining (Figures 6c and S12). Analysis shows that about 98% (SSEA1) and 95% (Oct4) of cells are iPSCs positive after FMSN incubation. Both the percentage of iPSCs that are stemness marker positive and the MFI of iPSCs are similar to those of the control. These results support the fact that FMSNs do not disturb the stemness of iPSCs. Moreover, quantitative reverse transcriptase polymerase chain reaction (qRT-PCR) was used to determine the messenger ribonucleic acid (mRNA) levels of iPSCs after FMSN uptake (Figure 6d). The results indicate that the mRNA levels of SSEA1 and Oct4 are similar to those of the control. These data also support the conclusion that the FMSNs

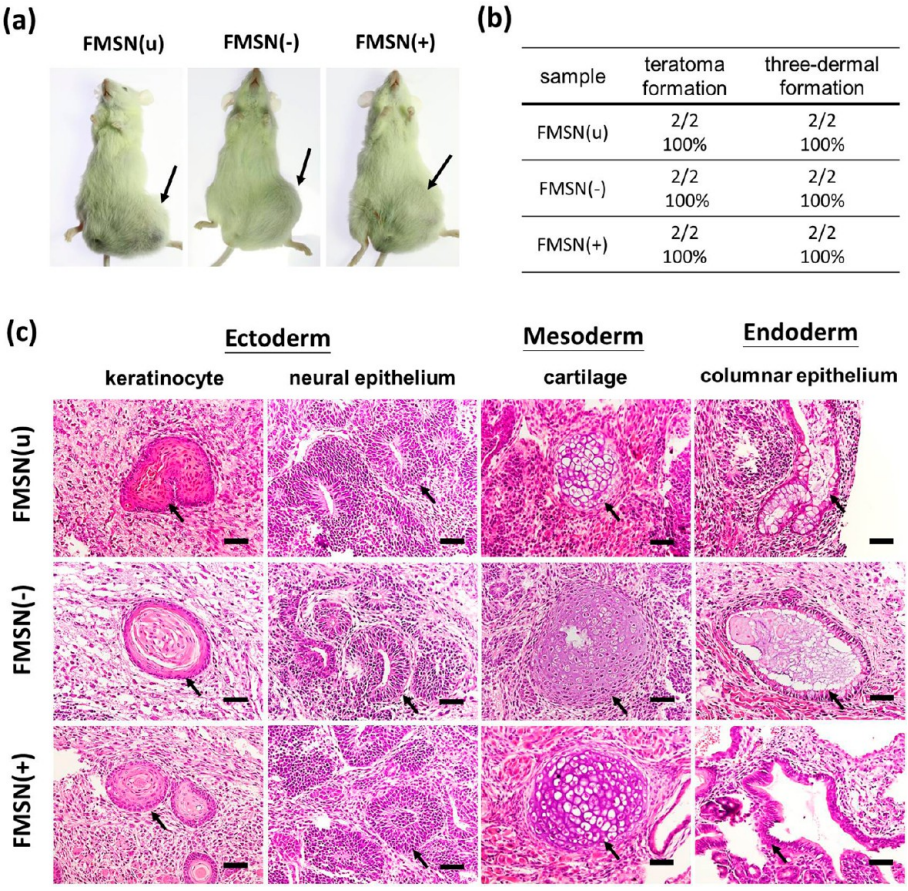

Figure 7. Teratoma formation analyses of immunodeficient NOD SCID mice. After incubation with 100 μg/mL FMSNs for 4 h, 3×10^6 iPSCs were subcutaneously injected in each mouse. (a) Photograph of NOD SCID mice. Seven weeks after iPSCs injection, the teratoma was easily observed. The arrows indicate the teratoma formation site. (b) Teratoma and three-dermal formation percentage analysis. Two mice for each type of nanoparticles were examined. (c) Examination of differentiation potential of iPSCs *in vivo*. The tissue sections were derived from teratoma and stained with hematoxylin and eosin. Three germ lineages are in each tissue including keratinocyte with keratin and neural epithelium (ectoderm), cartilage (mesoderm), and columnar epithelium (endoderm). Scale bars are 50 μm.

do not affect the pluripotent and stemness signatures, including Oct4 and SSEA1 (ES cell markers), in FMSN-treated iPSCs.

FMSNs Do Not Interfere with the Capability of Teratoma Formation of iPSCs *in Vivo*. It has been shown that iPSCs were indistinguishable from ES cells in morphology, surface antigens, gene expression, status of pluripotent cell-specific genes, and telomerase activity.[1] iPSCs share the same features as ES cells and are capable of pluripotency and differentiation into three germ layers.[2] The teratoma assay is one of the most common platforms for demonstrating the pluripotency and multidifferentiation of ES cells or iPSCs.[69,70] To investigate whether FMSNs could interfere with the pluripotency of iPSCs *in vivo*, we used the teratoma assay to demonstrate the differentiation potentials of FMSN-treated iPSCs in the transplanted grafts of immunocompromised mice. After the FMSNs were incubated, iPSCs were subcutaneously injected into immunodeficient NOD SCID mice, two mice per type of FMSN. After 7 weeks of injection, teratoma formation was easily observed (Figure 7a). Tissue slices were stained with hematoxylin and eosin. Three different germ layers, including typical keratinocyte-like and neural epithelium-like tissues (ectodermal lineage), cartilage-like tissues (mesodermal lineage), and columnar epithelium derived from endodermal-lineage tissues, were observed for the individual sample from all three groups (Figure 7b and c). After incubation with the three types of FMSNs, iPSCs still have the ability to differentiate into three different germ layers *in vivo*. Therefore, these results of the teratoma assay with histological survey supported that FMSNs would not interfere with the pluripotency and multidifferentiation potential of the iPSCs *in vivo*.

The leukemia inhibitory factor (LIF) is an important cytokine that supports maintenance of the self-renewing pluripotent state of mouse ES cells, as well as iPSCs.[71,72] When LIF is removed from ES cells or iPSC culture, the pluripotency of ES cells or iPSCs will be significantly decreased, and then the differentiation will proceed in ES cells or iPSCs.[72] We further explored whether FMSN could affect the differentiation ability and cell fate of iPSCs, especially under the LIF-removed

condition. Notably, under the differentiation condition of withdrawal of LIF and mouse embryonic fibroblast (MEF) cultivation, our data suggested that FMSN(u) and FMSN(+) present the potential to enhance the tridermal differentiation abilities of iPSCs, in part, through suppression of Oct4 and Nanog expression (Figures S13 and S14 and detailed discussion in the SI). This minimal effect on the differentiation of iPSCs by negatively charged nanoparticles is similar to the negative effect of carboxylate groups on the polymeric substrates for iPSCs and neuron differentiation.[73,74] Moreover, recent studies found that the excess amount of cationic charges of polycationic polymers may interfere with the cellular functions and physiology of biomacromolecules such as proteins and enzymes.[75,76] Notably, the excess cationic polymers might disrupt the function of the RNA-induced silencing complex and further influence the expression of Oct4. Notably, in Figure 2e, our data showed that the uptake of FMSN(u) and FMSN(+) in iPSCs, especially in FMSN(+), was significantly higher than that of FMSN(−), suggesting an excess of cationic charge with uptake may inhibit the stemness gene signature (Figure S13) and promote the activation of differentiation genes (Figure S14). Additionally, there are examples where nanomaterials affect the intracellular transport[77,78] and reports of signaling-active molecules inside endosomes.[79−81] This apparent promoting effect of FMSN(u) and FMSN(+) may be due to more uptake of these nanoparticles in iPSCs. Finally, the role of nanoparticles with different physical characteristics, such as FMSN(−), FMSN(+), and FMSN(u), in modulating the trans-activated stemness-gene signatures, pluripotency-related signal pathways, and differentiation lineage-specific target genes of adult stem cells, embryonic stem cells, and/or induced pluripotent stem cells could be investigated in the future.

pHNF3β-FMSN(+) Facilitates iPSC Differentiation into Hepatocyte-like Cells. Because of the multiple advantages of FMSNs to serve not only as ideal vectors for stem cells labeling but also as a high-efficient delivery platform to iPSCs, we then further explored the gene-transferring potential of pHNF3β-FMSN(+) (plasmid for hepatocyte nuclear factor 3β, pHNF3β) in regulating the differentiation of iPSCs toward endodermal and hepatic-specific cells (endoderm). HNF3β, a forkhead box transcription factor, is one of key transcription factors for liver development during mouse embryogenesis and is essential for the onset of hepatogenesis.[82,83] The pHNF3β was loaded on FMSN-(+) to form pHNF3β-FMSN(+) complexes by electrostatic adsorption. When the ratio of pHNF3β to FMSN(+) (w/w) was less than 1/16 (*i.e.*, FMSN(+) > 16), a stable complex was formed with no free pHNF3β detected by agarose gel electrophoresis (Figure S15a). Therefore, we chose pHNF3β to FMSN(+) ratios (w/w) of 1/16 and 1/128 (low and high amount of FMSN(+)) for the transduction studies. The pHNF3β-FMSN(+) complexes were characterized by their zeta potentials and DLS sizes in the DMEM (pH = 7.4, Figure S15b,c). The zeta potential became less negative with increasing amounts of FMSN(+), indicating the neutralization of the negative charge of pHNF3β had occurred and indirectly confirming the formation of the complexes. However, as the charge was near neutral (-5.5 ± 1.2 mV), aggregation occurred, leading to large DLS size for the 1/128 complex (705 ± 46 nm).

The iPSCs (Figure 8a, upper left) treated with pHNF3β-FMSN(+) and the controls (pHNF3β only, iPSCs only, and pHNF3β-Lipofectamine 2000 as a non-viral vector control) were cultivated in hepatic differentiation media. After 15 days, the control cells undergoing differentiation exhibited only slightly flattened cell morphology (Figure 8a, upper right). Compared with pHNF3β only (Figure 8a, lower left), our results showed that the treatment of pHNF3β-FMSN(+) 1/16 facilitated the differentiation of iPSCs into hepatocyte-like cells (iPSC-Heps), which displayed a cuboidal morphology with a large nucleus, a typical mark of hepatocytes, within 15 days of induction (Figure 8a, lower right). Normally, it takes 28 days for iPSC-Heps that received the standard differentiation to become mature iPSC-Heps.[14]

To further examine whether pHNF3β-FMSN(+) was able to promote the expression of liver-specific genes, we confirmed the mRNA-expression levels of liver genes by qRT-PCR. Notably, using FMSN(+) as a gene delivery platform, the data of qRT-PCR demonstrated that the ectopic-overexpression levels of HNF3β mRNA of iPSCs treated with pHNF3β-FMSN(+) 1/16 or pHNF3β-FMSN(+) 1/128 (Figure 8b) were significantly higher than those of control groups but not as high as that of the pHNF3β-Lipofectamine 2000 complex treated iPSCs (Figure 8b, upper left). Indeed, the transduction efficiency of the pHNF3β-FMSN(+) complex was slightly lower than that of the pHNF3β-Lipofectamine 2000 complex (Figure S16). Importantly, after induction of the hepatic differentiation for 15 days, the endogenous mRNA-expression levels of hepatocyte nuclear factor 4α (HNF4α; a specific visceral-endoderm gene),[84] albumin (ALB; a specific liver protein), and α-1-antitrypsin (AAT; a plasma serine protease inhibitor of liver)[85] were also up-regulated at iPSC-Heps treated with pHNF3β-FMSN(+), as compared with the control groups (Figure 8b). The mRNA-expression levels of AML12, a mouse hepatocyte cell line,[86] were included for reference in Figure 8b. Interestingly, the expression level of AAT in AML12 was quite low. Furthermore, immunofluorescence staining of the nuclear factors, HNF3β and HNF4α, in all groups is shown in Figure 9. iPSC-Heps treated with pHNF3β-FMSN(+) complexes (1/16 and 1/128) along with those treated with pHNF3β-Lipofectamine 2000 (positive control) and AML12 cells display bright and intense green HNF3β (Figure 9a) and red HNF4α (Figure 9b) images, yet dim or sporadic

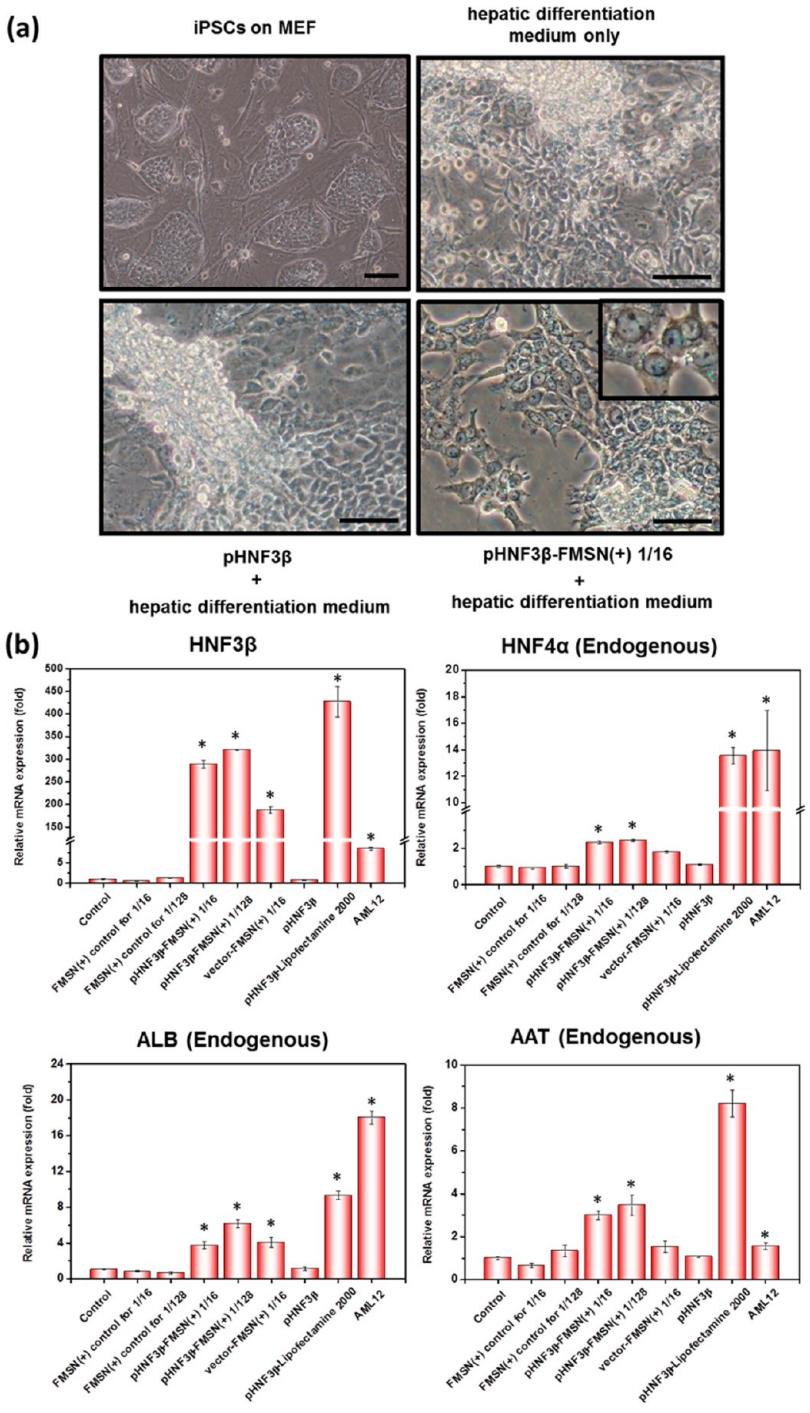

Figure 8. pHNF3β-FMSN(+) facilitated iPSCs differentiation toward definitive endodermal and hepatic lineage. (a) iPSCs cultivated on MEF formed the aggregated colony-like formation (upper left). Scale bars are 100 μm. *In vitro* iPSCs differentiated into hepatocyte-like cells (iPSC-Heps) under hepatic differentiation medium (100 ng/mL Activin A and 10 ng/mL basic fibroblast growth factor) for 15 days (upper right). iPSCs treated with pHNF3β only (lower left) or pHNF3β-FMSN(+) (lower right) were cultivated for 15 days under hepatic differentiation media. Scale bars are 100 μm. (b) Relative mRNA expression levels of iPSCs of endodermal or hepatic-lineage specific genes quantified by qRT-PCR after the vector-FMSN(+) or pHNF3β-FMSN(+) delivery in iPSCs. The iPSCs were transfected for 4 h and differentiated for 15 days. qRT-PCR analysis revealed the mRNA expression levels of hepatocyte-specific markers, including HNF3β, HNF4α, albumin (ALB), and α-1-antitrypsin (AAT), in iPSCs treated with vector-FMSN(+), pHNF3β-FMSN(+), or other control groups. pHNF3β-Lipofectamine 2000: liposomal transfection; positive control for transfection. AML12: a mouse hepatocyte cell line; positive control for mature hepatic cells. Data are means $\pm$ SD of three independent experiments. Asterisks indicate statistical differences ($p < 0.05$) compared with control.

green or red images were displayed by the controls. Therefore, more hepatic differentiation resulted from the nanoparticle-complex treatment, and FMSN(+) carrying pHNF3β can be an efficient platform to improve

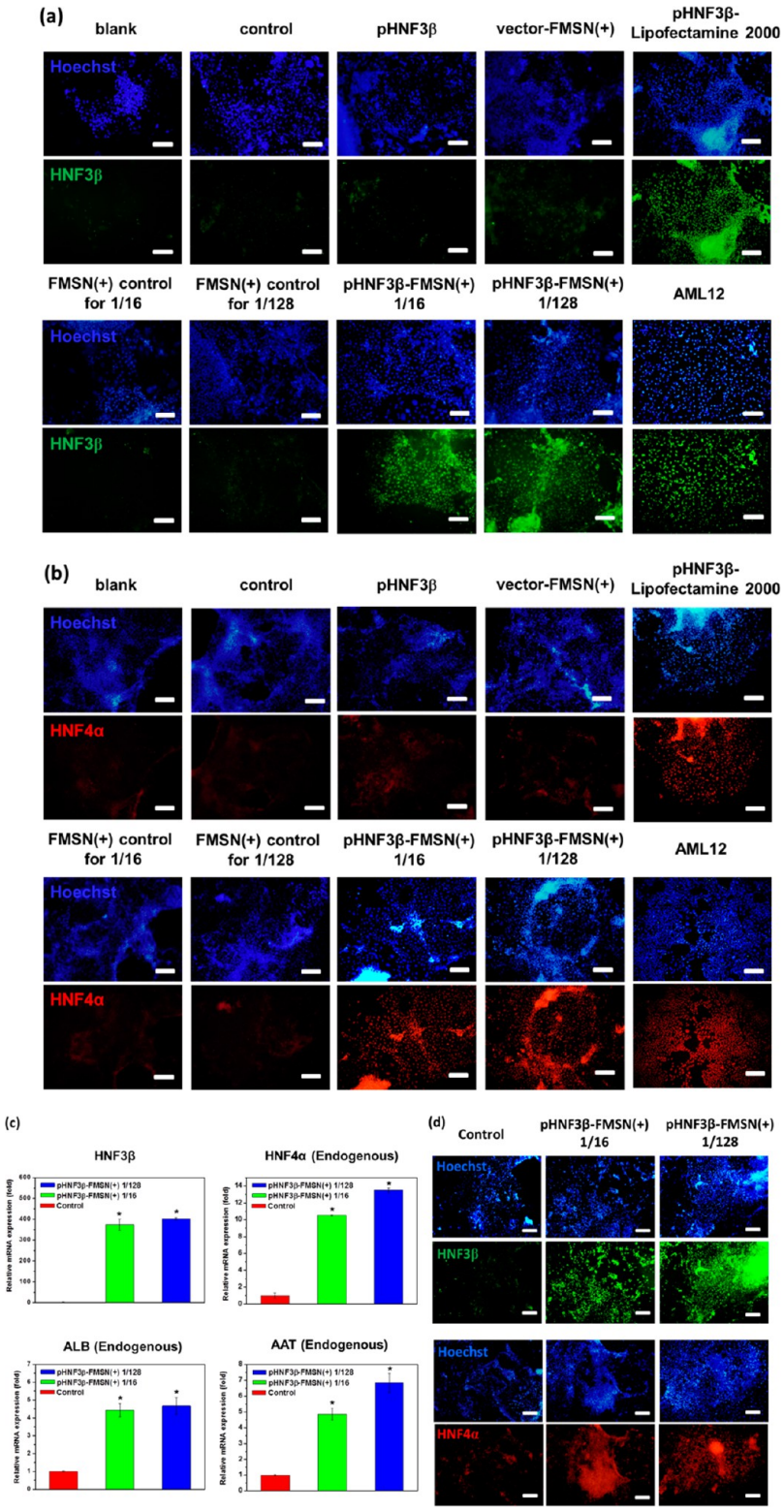

Figure 9. Immunofluorescence analysis for the expression of the hepatic markers HNF3β (green) and HNF4α (red) in pHNF3β-FMSN(+)-treated iPSCs and controls. iPSCs were grown for 15 days. Nuclei were counterstained with Hoechst 33342 (blue). pHNF3β-Lipofectamine 2000: liposomal transfection; positive control for transfection. AML12: a mouse hepatocyte cell line; positive control for mature hepatic cells. Scale bars are 200 μm. (c) Analysis of delivery of iPSCs with pHNF3β-FMSN(+) 1/16 and pHNF3β-FMSN(+) 1/128 on day 1 and day 3. Relative mRNA expression levels of iPSCs of endodermal or hepatic-lineage specific genes quantified by qRT-PCR. Asterisks indicate statistical differences ($p < 0.05$) compared with control. (d) Immunofluorescence staining of iPSCs treated with pHNF3β-FMSN(+) twice and stained with HNF3β and HNF4α antibodies. Scale bars are 200 μm.

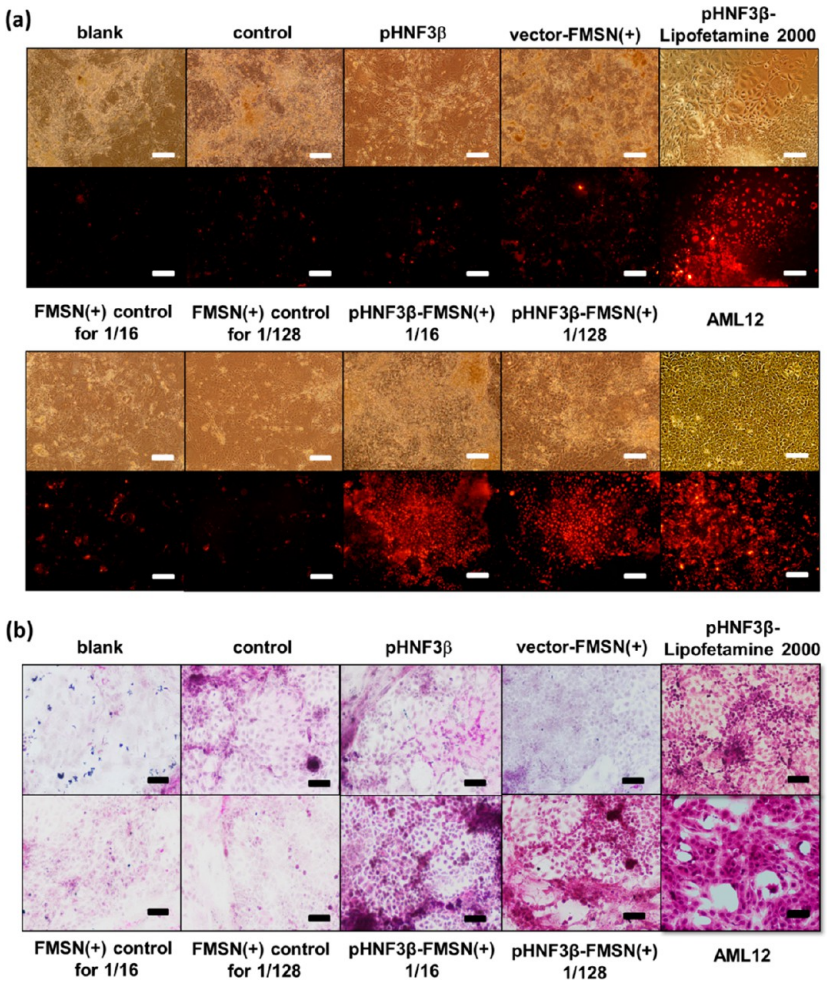

Figure 10. Analysis of LDL-uptake and glycogen-storage functions of iPSCs treated with pHNF3β-FMSN(+) or controls. (a) Functional test of hepatocyte-like cells (iPSC-Heps) after 4 h transduction and 15 days differentiation. The cells were examined for the ability to take up acetylated LDL, labeled with 1,1′-dioctadecyl-3,3,3′,3′-tetramethylindocarbocyanine perchlorate (red) for 24 h. The LDL uptake function of iPSC-Heps in the different treatment groups was analyzed by an immunofluorescent reaction and recorded using a fluorescence microscope. The blank indicates iPSCs were incubated in the absence of hepatic differentiation medium (100 ng/mL Activin A and 10 ng/mL basic fibroblast growth factor) for 15 days, while other groups were incubated with hepatic differentiation medium. pHNF3β-Lipofectamine 2000 delivery and AML12 (a cell line derived from hepatocytes) were included as positive controls. Scale bars are 200 μm. (b) The functions of glycogen synthesis and storage were measured by periodic acid-Schiff (PAS) staining (positive for glycogen; purple color) in iPSC-Heps in the different treatment groups. Scale bars are 200 μm.

definitive hepatic differentiation. It has been reported that multiple deliveries of different factors improve the efficiency of iPSC differentiation to hepatocyte cells.[15,16] We delivered pHNF3β on day 1 and 3 and differentiated for 15 days. Relative mRNA expression levels improved in this two-delivery study (Figure 9c,d). Therefore, these data suggest that FMSN(+) carrying pHNF3β can be an efficient nonviral gene-delivery system to improve definitive hepatic induction and promote the differentiation of iPSCs into iPSC-Heps.

Treatment with pHNF3β-FMSN(+) Promotes Hepatic Maturation and Liver-Uptake Function of iPSC-Heps. We further examined whether pHNF3β-FMSN(+) can promote hepatic differentiation with mature liver function in the treated iPSCs. Study assays for monitoring the abilities of low-density lipoprotein (LDL) uptake and glycogen storage were undertaken.[15] First, we monitored the abilities of LDL uptake by immunofluorescent imaging. In the control groups (Figure 10a), neither cellular uptake of LDL nor glycogen synthesis was observed in undifferentiated iPSCs. The positive immunofluorescent signals for LDL uptake in pHNF3β-FMSN(+)-treated groups increased significantly in the hepatic-lineage differentiation at day 15, as compared with those of other control groups (Figure 10a). AML12 was used as a positive differentiation control of mature hepatocytes for iPSC-Heps under different treatments. We also used liposomal transfection (Lipofectamine 2000) as a positive transfection control for the delivery efficiency of FMSNs. Moreover, the treatment effect of pHNF3β-FMSN(+) was similar to the two positive controls (Lipofectamine 2000 and AML12). Therefore, compared to the different controls and treatments, the results of the LDL-uptake analyses in iPSC-Heps also

support the idea that the treatment of pHNF3β-FMSN(+) can improve the hepatic maturation and liver-uptake function of iPSC-Heps. Meanwhile, similar findings were also made in the observation of large amounts of glycogen storage (another mature function of hepatocytes) of iPSC cells treated with pHNF3β-FMSN(+), as compared with those of the control groups (Figure 10b). Taken together, these data suggest that treatment of pHNF3β-FMSN(+) can not only promote iPSCs toward hepatic differentiation with high efficiency but also improve significantly the maturation of iPSC-Heps with liver-specific functions.

CONCLUSION

The discovery of iPSCs by Yamanaka revolutionized regenerative biology and presented great opportunities in medical fields.[1,2] Some of the proposed applications are in replacement therapy and pharmaceutical screening. Facile generation of hepatocytes from iPSCs can facilitate the development of replacement therapy and pharmaceutical screening in addition to establishing disease models. In this report, we have demonstrated that pHNF3β-FMSN(+) improved iPSC differentiation toward hepatocyte-like lineage with mature liver function, and double delivery of pHNF3β-FMSN(+) further improved mRNA-expression levels of liver-specific genes.

We have also demonstrated that mesoporous silica nanoparticles with various surface charges could be efficiently internalized by iPSCs without causing cytotoxicity. The levels of reactive oxygen species and pluripotent status, including *in vitro* stemness signatures and *in vivo* teratoma formation, remained unaltered. Therefore, FMSNs with multifunctional properties are suitable delivery platforms for biomolecule delivery and serve as an ideal vector for stem-cell labeling and gene delivery, as well as a potential drug for inducing specific differentiation and cell-oriented therapeutics.

MATERIALS AND METHODS

All chemicals were purchased from commercial suppliers (Acros, Aldrich, Sigma, and Merck) and were used without further purification.

Synthesis of FITC-Conjugated Mesoporous Silica Nanoparticles (FMSN(u)). FMSN(u) were synthesized following the methods in our previous reports.[18,41] Positively charged FMSN(+) was obtained by modifying the FMSN(u) surface with *N*-trimethoxysilylpropyl-*N*,*N*,*N*-trimethylammonium chloride before surfactant extraction. Sodium 3-trihydroxysilylpropylmethylphosphonate was used to obtain FMSN(−). Detailed synthesis and characterization are provided in the Supporting Information.

iPSC Generation and Culture. For reprogramming mouse fibroblast cells into iPSCs, mouse fibroblast cells were isolated from embryos of C57/B6 mice and cultured in Dulbecco's modified Eagle medium (Invitrogen, San Diego, CA, USA) supplemented with 10% fetal bovine serum (FBS, Invitrogen) at 37 °C, 5% CO_2. Mouse fibroblast cells were infected for 24 h with lentiviruses encoding the four reprogramming factors (Sox2, Klf4, c-Myc, and Oct4) in the presence of 8 ng/mL Polybrene, following the protocol described previously.[87] The culture medium was changed every other day, until background colonies emerged, after which the medium was changed daily. ES-like colonies appeared from large background colonies 7 days after viral transduction and were manually picked on days 24−30. Colonies that maintained their ES-like morphology were further passaged and analyzed for pluripotency potential.[70]

iPSCs were cultured on mitotically inactivated mouse embryonic fibroblasts (50 000 cells/cm^2) in DMEM supplemented with 15% FBS, 0.1 mM nonessential amino acids (Invitrogen, 11140-050), 0.55 mM 2-mercaptoethanol (Sigma, M7154-100 ML), 50 μg/mL penicillin−streptomycin (Invitrogen, 15140-122), and 0.3% recombinant leukemia inhibitory factor (Invitrogen, PMC9484) at 37 °C, 5% CO_2. In all culture conditions, the iPSC culture media were changed daily and cells were treated with trypsin (1 mg/mL, 5 min) or manually passaged every 3 or 4 days.

Cellular Uptake by Flow Cytometry. The iPSCs cellular uptake efficiency was determined by a flow cytometer (BD LSRFortessa cell analyzer, Becton Dickenson, Franklin Lakes, NJ, USA) and BD FACSDiva software (Becton Dickenson). The FITC dye in the FMSNs serves as a marker to determine the iPSC uptake efficiency. Before cell-seeding, the 12-well plates were coated with 0.1 wt % gelatin solution for 30 min, and the plates were washed with DMEM. iPSCs were seeded in 0.1% gelatin-coated 12-well plates with 1 mL of DMEM supplemented with 10% FBS and 1% penicillin−streptomycin at a cell density of 2×10^5 cells per well. After a 24 h incubation at 37 °C, the DMEM was replaced with 1 mL of FMSN(u) suspensions of various concentrations (0 (control), 25, 50, 85, and 100 μg/mL in DMEM), and the mixtures were incubated for various durations (0.5, 1, 2, and 4 h). The treated cells were washed twice with DMEM. Then, the cells were dispersed in 0.4 mL of PBS. Trypan blue was added to quench the extracellular FITC signals from the FMSN(u) attached on the cell surface, and flow cytometry analysis was carried out. The uptake of FMSN(−) and FMSN(+) for iPSCs was also evaluated by flow cytometry using the same procedures.

Inductively Coupled Plasma Mass Spectrometry (ICP-MS) Detection of FMSNs Uptake. After seeding, cells were incubated in DMEM with 100 μg/mL FMSNs for 4 h, and the iPSCs were washed with PBS three times and harvested by trypsinization. After trypsinization, iPSCs were washed twice and centrifuged to obtain cell pellets, which were digested with HF and HNO_3 to dissolve the FMSNs and iPSCs. The mass of FMSNs in the iPSCs was quantified by measuring the silicon concentration with ICP-MS.

Uptake Mechanism Experiments. To study the cellular uptake mechanism, iPSCs were preincubated at 37 °C with several pharmaceutical inhibitors: NaN_3 (5 mM, 1 h), 0.1 w/v % NaN_3 and 50 mM 2-deoxyglucose (1 h); sucrose (225 mM, 30 min); filipin (3 μg/mL, 1 h); cytochalasin D (3 μg/mL, 30 min); and nocodazole (30 μM, 30 min). Afterward, iPSCs were co-incubated with 100 μg/mL FMSNs for 4 h. The iPSCs were washed with PBS three times and harvested by trypsinization for flow cytometry examination.

Exocytosis Mechanism Experiments. After incubation with 100 μg/mL FMSNs for 4 h, iPSCs were washed, harvested, and recultured in DMEM supplemented with 10% FBS and 1% penicillin−streptomycin. Then, iPSCs were cultured in 113 mM sucrose or 3 μg/mL filipin in a DMEM solution supplemented with 10% FBS and 1% penicillin−streptomycin. After 18 and 42 h, the iPSCs were washed with PBS three times and harvested by trypsinization for flow cytometry examination.

Cellular Cytotoxicity. The viability of FMSNs against iPSCs was evaluated by a colorimetric WST-1 assay. The cells were seeded in 24-well plates at a seeding density of 2×10^4 cells per well in 0.5 mL of DMEM supplemented with 10% FBS and 1% penicillin−streptomycin at 37 °C for 24 h attachment. After the attachment, the medium was removed and the cells were incubated in 0.5 mL of fresh DMEM containing 0, 12.5, 25, 50, 75, and 100 μg of FMSNs (*i.e.*, 0, 25, 50, 100, 150, and 200 μg/mL, respectively) for 4 or 24 h at 37 °C. After incubation, the medium

was removed and the treated cells were washed twice with fresh DMEM. To investigate the cell viability, 200 μL of DMEM and 20 μL of premixed WST-1 cellular cytotoxicity reagent (containing WST-1 and an electron-coupling reagent, diluted in sterile phosphate buffer saline) were added to each well. Afterward, the 24-well plate was shaken thoroughly for 1 min and left in the incubator for 4 h at 37 °C. Finally, 100 μL of the reaction solution from each well was transferred to a 96-well plate. A 96-well plate ELISA reader from Bio-Rad was used to measure the absorbance at 450 and 655 nm (a reference) simultaneously. The culture medium with premixed WST-1 reagent was defined as a background control.

The cellular proliferation of FMSNs against iPSCs was evaluated by a colorimetric WST-1 assay. After seeding, medium was removed and the cells were incubated in 0.5 mL of fresh DMEM containing 0, 25, and 50 μg of FMSNs (*i.e.*, 0, 50, and 100 μg/mL, respectively) for 4 h in the incubator at 37 °C. Afterward, the cells were allowed to grow in 0.5 mL of fresh DMEM supplemented with 10% FBS and 1% penicillin−streptomycin for 40 h. For cell proliferation, the examination procedure is the same as that of the WST-1 viability assay described above.

In addition, the cellular integrity of iPSCs after FMSN incubation was evaluated by a lactate dehydrogenase assay. Typically, 0.1 mL of nicotinamide adenine dinucleotide, 0.1 mL of lactic acid, 0.1 mL of tetrazolium salt, and 0.1 mL of reconstituted diaphorase were added to a 9.6 mL LDH assay buffer to prepare the LDH reaction solution. After seeding, the medium was removed and the cells were incubated in 0.5 mL of fresh Roswell Park Memorial Institute (RPMI) 1640 medium containing 0, 12.5, 25, 50, 75, and 100 μg of FMSN nanoparticles for 4 h at 37 °C. After incubation, the cell medium was centrifuged, and 100 μL of the supernatant was added to 100 μL of LDH reaction solution in a 96-well plate. The mixture was shaken for 30 min at RT. To determine the amount of LDH, a multiwell plate ELISA reader from Bio-Rad was used to measure the absorbance at 490 and 690 nm (as a reference) simultaneously. The LDH reaction solution with culture medium only (without cells) was defined as a background control.

Immunofluorescence Staining. For immunostaining, iPSCs were seeded on a 0.1% gelatin coated chamber slide for 24 h and incubated in 1 mL of FMSN suspension at a concentration of 100 μg/mL in DMEM for 4 h. After incubation, the iPSCs were washed with PBS, fixed with 4% paraformaldehyde, and then permeabilized with 0.1% IGEPAL CA-630. Cells were incubated with mouse or rabbit monoclonal antibodies against SSEA1 (Cell Signaling, #4744) or Oct4 (Cell Signaling, #2840) at appropriate dilution overnight at 4 °C. After that, cells were washed extensively with PBS and treated with DyLight594-conjugated corresponding secondary antibodies (Jackson ImmunoResearch, West Grove, PA, USA) and counterstained with Hoechst 33342 (Sigma) before being visualized under an Olympus confocal microscope.

Stemness Marker Determination. The iPSCs incubated with FMSNs were harvested 4 h postincubation. iPSCs were treated with a mixture of trypsin and ethylenediaminetetraacetic acid and washed with PBS. Following trypsinization and centrifugation of cells, the cell pellet was resuspended in staining solution containing 0.1% bovine serum albumin (BSA, Invitrogen) in PBS. For SSEA1 staining, cells were stained with anti-SSEA1 antibody (Cell Signaling, #4744) for 30 min on ice and then washed with PBS containing 0.1% BSA. After that, DyLight594-conjugated secondary antibody was added to both the isotype control and the SSEA1-stained cells, and cells were incubated on ice for 30 min. For Oct4 staining of iPSCs, cells were fixed with 4% paraformaldehyde, permeabilized with 0.1% IGEPAL CA-630, and then washed with PBS containing 0.1% BSA. After that, anti-Oct4 antibody (Cell Signaling, #2840) was added and incubated with cells on ice for 30 min. Cells were then washed with staining solution, and secondary antibody conjugated to DyLight594 was added and incubated for 30 min on ice. Labeled cells were washed, and cells were resuspended in 0.5 mL of PBS containing 0.1% BSA. The populations of labeled cells were evaluated by flow cytometry.

Quantitative Reverse Transcriptase Polymerase Chain Reaction. qRT-PCR was used to examine and quantify the gene expression levels in iPSCs. After seeding, the iPSCs were incubated in DMEM containing 100 μg/mL FMSNs in six-well plates for 4 h. After incubation, the cells were washed with DMEM twice and grown in the DMEM supplemented with 10% FBS.

After being further cultured for 5 and 11 days, total RNA from cultured cells was extracted using Trizol reagent (Invitrogen). In brief, 1 mL of Trizol reagent was added to homogenize the cell lysate, and the reaction mixture was incubated for 5 min at room temperature (RT). Then 0.2 mL of chloroform was added, and the mixture was centrifuged (12000*g*, 15 min, RT) to separate the two phases. The colorless aqueous phase was transferred to a fresh tube, and 0.5 mL of isopropyl alcohol (Sigma-Aldrich, St. Louis, MO, USA) was added. Ten minutes later, the precipitate was collected by centrifugation at 16000*g* for 10 min at 4 °C. The pellet was then washed with 1 mL of 75% ethanol. After ethanol was completely removed, the pellet was dissolved in 30 μL of diethylpyrocarbonate-treated H_2O (Life Technologies, Carlsbad, CA, USA).

The total RNA was estimated by UltroSpec 3100 Pro (Amersham). A 1 μg amount of RNA was reversely transcribed with a SuperScript III reverse transcriptase kit (Invitrogen) following the manufacturer's manual. Quantitative PCR analysis was performed in real time using an ABI 7900 Fast System and SYBR Green Master Mix. Conditions for PCR amplifications were as follows: 94 °C for 3 min, 35 thermal cycles (denaturing the DNA at 94 °C for 30 s, annealing with the primer at 60 °C for 5 s, extending the length of product at 72 °C for 1 min), and a final extension at 72 °C for 10 min. Reactions were carried out by using specific primers listed in the Supporting Information (Table S2). For quantitation, the raw data were normalized to glyceraldehyde 3-phosphate dehydrogenase (Gapdh). Error bars indicate standard deviation of triplicate measurements.

Teratoma Formation Examination. This study was approved by Taipei Veterans General Hospital Animal Committee, and the principles of Laboratory Animal Care were followed. Only male NOD SCID mice were used in the transplantation studies. iPSCs were treated with FMSNs (100 μg/mL, 4 h). Cells were suspended at 1×10^7 cells/mL in PBS. We subcutaneously transplanted 3×10^6 cells into 3- to 4-week-old NOD SCID mice ($n = 2$, FMSN(u), FMSN(+), and FMSN(−)). Seven weeks after the injection, teratoma was surgically dissected for histological analysis. Samples were fixed in PBS containing 4% formaldehyde and embedded in paraffin. Sections were stained with hematoxylin and eosin.

Evaluation of Intracellular Reactive Oxygen Species. Intracellular ROS level was evaluated using the fluorescent probe dihydroethidium (DHE, Invitrogen). After the FMSN incubation (100 μg/mL, 4 h), cells were incubated with DHE at a concentration of 2 μM for another 30 min at 37 °C. The intracellular ROS were quantified by flow cytometry.

Plasmid Construction. The mammalian plasmid can be used in transiently expressing genes by transfection. The EF1α promoters allow ectopic genes to achieve robust and constitutive expression in mammalian cells. We introduced HNF3β cDNA, isolated from pCMV-Sport6-HNF3β, into pLV-EF1α-IRES (vector) at the sites of *Bam*HI/ApaI. The construction of pLV-EF1α-HNF3β-IRES (plasmid HNF3β, pHNF3β) and pLV-EF1α-HNF3β-IRES-RFP (pHNF3β(RFP)) was confirmed by direct sequencing. The pHNF3β was transformed and amplified into the DH5α *E. coli* strain. The pHNF3β was purified using an Invitrogen Maxi plasmid preparation kit (Life Technologies), and the manufacturer's instructions were followed. The concentration and purity of pHNF3β were measured by ultraviolet (UV) absorbance at 260 and 280 nm, respectively. pHNF3β was used for induction of hepatic differentiation in iPSCs. The transduction of pHNF3β(RFP) enables iPSCs to produce red fluorescent protein whereby the FMSN-delivery efficiency can be estimated by fluorescence microscope and flow cytometry.

pHNF3β-FMSN(+) Binding and Agarose Gel Electrophoresis. One microgram of pHNF3β was mixed with various amounts of FMSN(+) at weight ratios (pHNF3β/FMSN(+)) of 1/1, 1/2, 1/4, 1/8, 1/16, 1/32, and 1/64 in DMEM. After 30 min incubation, pHNF3β-FMSN(+) complexes were loaded onto the 1.0% agarose gel. After gel electrophoresis (110 V for 30 min), DNA bands were visualized by ethidium bromide staining. Naked pHNF3β, FMSN(+), and size standards were used as references.

iPSC Transduction and *in Vitro* Hepatic Differentiation. Before the induction of hepatic differentiation, iPSCs were trypsinized into single cells and suspended in a mouse ES medium without LIF. The iPSC colonies were cultured in suspension in uncoated Petri dishes for 4 days to collect embryoid bodies. Embryoid bodies were plated onto gelatin-coated six-well plates. For induction of hepatocytes, delivery of the pHNF3β-FMSN(+) complex was carried out by adding 34 and 258 μg of pHNF3β-FMSN(+) complexes (pHNF3β/FMSN(+) = 1/16 and 1/128) into 2 mL of DMEM, respectively. In addition, incubation with pHNF3β only (2 μg), FMSN(+) only (32 μg, 256 μg for FMSN(+) control for 1/16 and 1/128, respectively), and 34 μg of vector-FMSN(+) (vector(pLV-EF1α-IRES)/FMSN(+) 1/16) was carried out separately for references. Moreover, Lipofectamine 2000 (Invitrogen) was used as a nonviral positive control. Similarly, 2 μg of pHNF3β and 6 μL of Lipofectamine 2000 were incubated in 100 μL of DMEM for 30 min. The complex was added to six-well plates containing 1.9 mL of DMEM and iPSC embryoid bodies. For all groups, the incubation time was 4 h. After washing with PBS, iPSCs were cultured in DMEM supplemented with 10% FBS, 100 ng/mL Activin A (R&D Systems), and 10 ng/mL basic fibroblast growth factor (bFGF, R&D Systems). In addition, iPSCs incubated in the absence of hepatic differentiation media (100 ng/mL Activin A and 10 ng/mL basic fibroblast growth factor) served as a blank. To observe long-term effects, iPSCs were cultured for 15 days. The culture medium was replaced with a freshly prepared medium every other day.

For the double-transduction experiment, on days 1 and 3, 34 and 258 μg of pHNF3β-FMSN(+) complexes (pHNF3β/FMSN(+) = 1/16 and 1/128) in 2 mL of DMEM were incubated with iPSCs (4 h), respectively. After washing with PBS, iPSCs were cultured as the single-transduction experiment described above, and total culture time was 15 days.

qRT-PCR Evaluation of Hepatocyte-like Cells. qRT-PCR was used to examine and quantify the gene expression levels in iPSC-Heps. After the iPSCs were transducted with pHNF3β-FMSN(+) and cultured for another 15 days, Trizol reagent was added to homogenize the iPSCs lysate. The RNA extraction, reverse-transcription, and quantitation procedures were the same as described above for qRT-PCR. The specific primers for hepatocyte-associated genes are listed in the Supporting Information (Table S2).

Immunofluorescence Staining of Hepatocyte-like Cells. Immunofluorescence staining was used to detect the presence of hepatic markers HNF3β and HNF4α in iPSC-Heps. Under the differentiation protocol, pHNF3β-FMSN(+)-transduced iPSCs were cultured for another 15 days. The iPSC-Heps were washed with PBS, fixed with 4% paraformaldehyde, and then permeabilized with 0.1% IGEPAL CA-630. The iPSC-Heps were subsequently incubated with primary antibody against HNF3β and HNF4α overnight. After that, cells were washed with PBS and treated with fluorescence-conjugated corresponding secondary antibodies. The iPSC-Heps sample was observed under an Olympus microscope.

Periodic Acid-Schiff Staining and Low-Density Lipoprotein Uptake Examination. For functional assessment of the hepatocyte-like cells (iPSC-Heps), periodic acid-Schiff staining and low-density lipoprotein uptake were employed. After the iPSCs were transducted with pHNF3β-FMSN(+) and cultured for another 15 days, iPSC-Heps were fixed in formalin−ethanol fixative solution (37% formaldehyde−95% ethanol, 1:9 (v/v)) and permeabilized with 0.1% Triton X-100 for 10 min. Samples were then oxidized in 1% periodic acid for 5 min, rinsed with deionized H_2O (dH_2O) three times, treated with Schiff's reagent for 15 min, and rinsed with dH_2O for 10 min. Samples were counterstained with Mayer's hematoxylin for 1 min, rinsed with dH_2O for 10 min, and assessed under a light microscope.

For LDL analysis, the iPSCs were transducted with pHNF3β-FMSN(+) and cultured for another 15 days. iPSC-Heps were incubated in DMEM containing 20 μg/mL acetylated low-density lipoprotein, labeled with 1,1′-dioctadecyl-3,3,3′,3′-tetramethylindocarbocyanine perchlorate (Dil-Ac-LDL, Biomedical Technologies, Stoughton, MA), for 24 h at 37 °C. iPSC-Heps were washed twice with PBS and visualized by fluorescence microscopy.

The same procedure was followed for Lipofectamine 2000 and AML 12.

Conflict of Interest: The authors declare no competing financial interest.

Supporting Information Available: Procedures for the synthesis and characterization of FMSNs, co-localization image of FMSNs and FM4-64, proliferation of mouse ES cells, N_2-sorption isotherms, dynamic light scattering, zeta potentials, fluorescence spectra, uptake flow cytometry data, mRNA level, stemness markers quantification, differentiation study, gel electrophoresis, gene delivery efficiency, and sequences of primers in RT-PCR and results in Figures S1 to S16 and Tables S1 and S2 are available free of charge *via* the Internet at http://pubs.acs.org.

Acknowledgment. This work was supported by the National Science Council of Taiwan under grants 99-2120-M-002-008 and 100-2120-M-002-011. We thank S. J. Chou and P. Y. Huang for maintaining iPSCs and M. L. Tsai for animal experiments.

REFERENCES AND NOTES

1. Takahashi, K.; Yamanaka, S. Induction of Pluripotent Stem Cells from Mouse Embryonic and Adult Fibroblast Cultures by Defined Factors. *Cell* **2006**, *126*, 663–676.
2. Takahashi, K.; Tanabe, K.; Ohnuki, M.; Narita, M.; Ichisaka, T.; Tomoda, K.; Yamanaka, S. Induction of Pluripotent Stem Cells from Adult Human Fibroblasts by Defined Factors. *Cell* **2007**, *131*, 861–872.
3. Corti, S.; Locatelli, F.; Papadimitriou, D.; Strazzer, S.; Bonato, S.; Comi, G. P. Nuclear Reprogramming and Adult Stem Cell Potential. *Histol. Histopathol.* **2005**, *20*, 977–986.
4. Park, I. H.; Zhao, R.; West, J. A.; Yabuuchi, A.; Huo, H.; Ince, T. A.; Lerou, P. H.; Lensch, M. W.; Daley, G. Q. Reprogramming of Human Somatic Cells to Pluripotency with Defined Factors. *Nature* **2008**, *451*, 141–146.
5. Yu, J.; Vodyanik, M. A.; Smuga-Otto, K.; Antosiewicz-Bourget, J.; Frane, J. L.; Tian, S.; Nie, J.; Jonsdottir, G. A.; Ruotti, V.; Stewart, R.; *et al*. Induced Pluripotent Stem Cell Lines Derived from Human Somatic Cells. *Science* **2007**, *318*, 1917–1920.
6. Lowry, W. E.; Richter, L.; Yachechko, R.; Pyle, A. D.; Tchieu, J.; Sridharan, R.; Clark, A. T.; Plath, K. Generation of Human Induced Pluripotent Stem Cells from Dermal Fibroblasts. *Proc. Natl. Acad. Sci. U.S.A.* **2008**, *105*, 2883–2888.
7. Danwei, H.; Osafune, K.; Maehr, R.; Guo, W.; Eijkelenboom, A.; Chen, S.; Muhlestein, W.; Melton, D. A. Induction of Pluripotent Stem Cells from Primary Human Fibroblasts with Only Oct4 and Sox2. *Nat. Biotechnol.* **2008**, *26*, 1269–1275.
8. Jesus Tunon, M.; Alvarez, M.; Culebras, J. M.; Gonzalez-Gallego, J. An Overview of Animal Models for Investigating the Pathogenesis and Therapeutic Strategies in Acute Hepatic Failure. *World J. Gastroenterol.* **2009**, *15*, 3086–3098.
9. Lee, W. M. Medical Progress-Acute Liver Failure. *New Engl. J. Med.* **1993**, *329*, 1862–1872.
10. Nussler, A.; Konig, S.; Ott, M.; Sokal, E.; Christ, B.; Thasler, W.; Brulport, M.; Gabelein, G.; Schormann, W.; Schulze, M.; *et al*. Present Status and Perspectives of Cell-Based Therapies for Liver Diseases. *J. Hepatol.* **2006**, *45*, 144–159.
11. Chen, Y. F.; Tseng, C. Y.; Wang, H. W.; Kuo, H. C.; Yang, V. W.; Lee, O. K. Rapid Generation of Mature Hepatocyte-Like Cells from Human Induced Pluripotent Stem Cells by an Efficient Three-Step Protocol. *Hepatology* **2012**, *55*, 1193–1203.
12. Rashid, S. T.; Corbineau, S.; Hannan, N.; Marciniak, S. J.; Miranda, E.; Alexander, G.; Huang-Doran, I.; Griffin, J.; Ahrlund-Richter, L.; Skepper, J.; *et al*. Modeling Inherited Metabolic Disorders of the Liver Using Human Induced Pluripotent Stem Cells. *J. Clin. Invest.* **2010**, *120*, 3127–3136.
13. Lapasset, L.; Milhavet, O.; Prieur, A.; Besnard, E.; Babled, A.; Ait-Hamou, N.; Leschik, J.; Pellestor, F.; Ramirez, J.-M.; De Vos, J.; *et al*. Rejuvenating Senescent and Centenarian Human Cells by Reprogramming through the Pluripotent State. *Gene Dev.* **2011**, *25*, 2248–2253.

14. Li, H. Y.; Chien, Y.; Chen, Y. J.; Chen, S. F.; Chang, Y. L.; Chiang, C. H.; Jeng, S. Y.; Chang, C. M.; Wang, M. L.; Chen, L. K.; *et al*. Reprogramming Induced Pluripotent Stem Cells in the Absence of c-Myc for Differentiation into Hepatocyte-Like Cells. *Biomaterials* **2011**, *32*, 5994–6005.
15. Takayama, K.; Inamura, M.; Kawabata, K.; Katayama, K.; Higuchi, M.; Tashiro, K.; Nonaka, A.; Sakurai, F.; Hayakawa, T.; Furue, M. K.; *et al*. Efficient Generation of Functional Hepatocytes from Human Embryonic Stem Cells and Induced Pluripotent Stem Cells by HNF4α Transduction. *Mol. Ther.* **2012**, *20*, 127–137.
16. Takayama, K.; Inamura, M.; Kawabata, K.; Sugawara, M.; Kikuchi, K.; Higuchi, M.; Nagamoto, Y.; Watanabe, H.; Tashiro, K.; Sakurai, F.; *et al*. Generation of Metabolically Functioning Hepatocytes from Human Pluripotent Stem Cells by FOXA2 and HNF1α Transduction. *J. Hepatol.* **2012**, *57*, 628–636.
17. Lu, J.; Liong, M.; Li, Z.; Zink, J. I.; Tamanoi, F. Biocompatibility, Biodistribution, and Drug-Delivery Efficiency of Mesoporous Silica Nanoparticles for Cancer Therapy in Animals. *Small* **2010**, *6*, 1794–1805.
18. Chung, T. H.; Wu, S. H.; Yao, M.; Lu, C. W.; Lin, Y. S.; Hung, Y.; Mou, C. Y.; Chen, Y. C.; Huang, D. M. The Effect of Surface Charge on the Uptake and Biological Function of Mesoporous Silica Nanoparticles in 3T3-L1 Cells and Human Mesenchymal Stem Cells. *Biomaterials* **2007**, *28*, 2959–2966.
19. Lu, C. W.; Hung, Y.; Hsiao, J. K.; Yao, M.; Chung, T. H.; Lin, Y. S.; Wu, S. H.; Hsu, S. C.; Liu, H. M.; Mou, C. Y.; *et al*. Bifunctional Magnetic Silica Nanoparticles for Highly Efficient Human Stem Cell Labeling. *Nano Lett.* **2007**, *7*, 149–154.
20. Zhao, Y.; Trewyn, B. G.; Slowing, I. I.; Lin, V. S. Y. Mesoporous Silica Nanoparticle-Based Double Drug Delivery System for Glucose-Responsive Controlled Release of Insulin and Cyclic AMP. *J. Am. Chem. Soc.* **2009**, *131*, 8398–8400.
21. Tu, H. L.; Lin, Y. S.; Lin, H. Y.; Hung, Y.; Lo, L. W.; Chen, Y. F.; Mou, C. Y. *In Vitro* Studies of Functionalized Mesoporous Silica Nanoparticles for Photodynamic Therapy. *Adv. Mater.* **2009**, *21*, 172–177.
22. Chen, Y. P.; Chen, C. T.; Hung, Y.; Chou, C. M.; Liu, T. P.; Liang, M. R.; Chen, C. T.; Mou, C. Y. A New Strategy for Intracellular Delivery of Enzyme Using Mesoporous Silica Nanoparticles: Superoxide Dismutase. *J. Am. Chem. Soc.* **2013**, *135*, 1516–1523.
23. Lin, Y. S.; Abadeer, N.; Hurley, K. R.; Haynes, C. L. Ultrastable, Redispersible, Small, and Highly Organomodified Mesoporous Silica Nanotherapeutics. *J. Am. Chem. Soc.* **2011**, *133*, 20444–20457.
24. Wu, S. H.; Hung, Y.; Mou, C. Y. Mesoporous Silica Nanoparticles as Nanocarriers. *Chem. Commun.* **2011**, *47*, 9972–9985.
25. Yuan, Q.; Zhang, Y.; Chen, T.; Lu, D.; Zhao, Z.; Zhang, X.; Li, Z.; Yan, C. H.; Tan, W. Photon-Manipulated Drug Release from a Mesoporous Nanocontainer Controlled by Azobenzene-Modified Nucleic Acid. *ACS Nano* **2012**, *6*, 6337–6344.
26. Thomas, C. R.; Ferris, D. P.; Lee, J. H.; Choi, E.; Cho, M. H.; Kim, E. S.; Stoddart, J. F.; Shin, J. S.; Cheon, J.; Zink, J. I. Noninvasive Remote-Controlled Release of Drug Molecules *in Vitro* Using Magnetic Actuation of Mechanized Nanoparticles. *J. Am. Chem. Soc.* **2010**, *132*, 10623–10625.
27. Lin, Y. S.; Hurley, K. R.; Haynes, C. L. Critical Considerations in the Biomedical Use of Mesoporous Silica Nanoparticles. *J. Phys. Chem. Lett.* **2012**, *3*, 364–374.
28. He, Q.; Gao, Y.; Zhang, L.; Zhang, Z.; Gao, F.; Ji, X.; Li, Y.; Shi, J. A pH-Responsive Mesoporous Silica Nanoparticles-Based Multi-Drug Delivery System for Overcoming Multi-Drug Resistance. *Biomaterials* **2011**, *32*, 7711–7720.
29. Zhao, Y. L.; Li, Z. X.; Kabehie, S.; Botros, Y. Y.; Stoddart, J. F.; Zink, J. I. pH-Operated Nanopistons on the Surfaces of Mesoporous Silica Nanoparticles. *J. Am. Chem. Soc.* **2010**, *132*, 13016–13025.
30. Li, Z.; Barnes, J. C.; Bosoy, A.; Stoddart, J. F.; Zink, J. I. Mesoporous Silica Nanoparticles in Biomedical Applications. *Chem. Soc. Rev.* **2012**, *41*, 2590–2605.
31. Meng, H.; Xue, M.; Xia, T.; Ji, Z.; Tarn, D. Y.; Zink, J. I.; Nel, A. E. Use of Size and a Copolymer Design Feature to Improve the Biodistribution and the Enhanced Permeability and Retention Effect of Doxorubicin-Loaded Mesoporous Silica Nanoparticles in a Murine Xenograft Tumor Model. *ACS Nano* **2011**, *5*, 4131–4144.
32. Slowing, I. I.; Trewyn, B. G.; Lin, V. S. Y. Mesoporous Silica Nanoparticles for Intracellular Delivery of Membrane-Impermeable Proteins. *J. Am. Chem. Soc.* **2007**, *129*, 8845–8849.
33. Wang, L.; Zhao, W.; Tan, W. Bioconjugated Silica Nanoparticles: Development and Applications. *Nano Res.* **2008**, *1*, 99–115.
34. Erathodiyil, N.; Ying, J. Y. Functionalization of Inorganic Nanoparticles for Bioimaging Applications. *Acc. Chem. Res.* **2011**, *44*, 925–935.
35. Meng, H.; Liong, M.; Xia, T.; Li, Z.; Ji, Z.; Zink, J. I.; Nel, A. E. Engineered Design of Mesoporous Silica Nanoparticles to Deliver Doxorubicin and P-Glycoprotein siRNA to Overcome Drug Resistance in a Cancer Cell Line. *ACS Nano* **2010**, *4*, 4539–4550.
36. Xia, T.; Kovochich, M.; Liong, M.; Meng, H.; Kabehie, S.; George, S.; Zink, J. I.; Nel, A. E. Polyethyleneimine Coating Enhances the Cellular Uptake of Mesoporous Silica Nanoparticles and Allows Safe Delivery of siRNA and DNA Constructs. *ACS Nano* **2009**, *3*, 3273–3286.
37. Gao, Y.; Chen, Y.; Ji, X.; He, X.; Yin, Q.; Zhang, Z.; Shi, J.; Li, Y. Controlled Intracellular Release of Doxorubicin in Multidrug-Resistant Cancer Cells by Tuning the Shell-Pore Sizes of Mesoporous Silica Nanoparticles. *ACS Nano* **2011**, *5*, 9788–9798.
38. Hsiao, J. K.; Tsai, C. P.; Chung, T. H.; Hung, Y.; Yao, M.; Liu, H. M.; Mou, C. Y.; Yang, C. S.; Chen, Y. C.; Huang, D. M. Mesoporous Silica Nanoparticles as a Delivery System of Gadolinium for Effective Human Stem Cell Tracking. *Small* **2008**, *4*, 1445–1452.
39. Lu, F.; Wu, S. H.; Hung, Y.; Mou, C. Y. Size Effect on Cell Uptake in Well-Suspended, Uniform Mesoporous Silica Nanoparticles. *Small* **2009**, *5*, 1408–1413.
40. Pagliari, F.; Mandoli, C.; Forte, G.; Magnani, E.; Pagliari, S.; Nardone, G.; Licoccia, S.; Minieri, M.; Di Nardo, P.; Traversa, E. Cerium Oxide Nanoparticles Protect Cardiac Progenitor Cells from Oxidative Stress. *ACS Nano* **2012**, *6*, 3767–3775.
41. Lin, Y. S.; Tsai, C. P.; Huang, H. Y.; Kuo, C. T.; Hung, Y.; Huang, D. M.; Chen, Y. C.; Mou, C. Y. Well-Ordered Mesoporous Silica Nanoparticles as Cell Markers. *Chem. Mater.* **2005**, *17*, 4570–4573.
42. Ruan, J.; Shen, J.; Wang, Z.; Ji, J. J.; Song, H.; Wang, K.; Liu, B.; Li, J. H.; Cui, D. X. Efficient Preparation and Labeling of Human Induced Pluripotent Stem Cells by Nanotechnology. *Int. J. Nanomed.* **2011**, *6*, 425–435.
43. Lee, C. H.; Kim, J. H.; Lee, H. J.; Jeon, K.; Lim, H.; Choi, H. Y.; Lee, E. R.; Park, S. H.; Park, J. Y.; Hong, S.; *et al*. The Generation of iPS Cells Using Non-Viral Magnetic Nanoparticle Based Transfection. *Biomaterials* **2011**, *32*, 6683–6691.
44. Chen, Y. P.; Chen, H. A.; Hung, Y.; Chien, F. C.; Chen, P. L.; Mou, C. Y. Surface Charge Effect in Intracellular Localization of Mesoporous Silica Nanoparticles as Probed by Fluorescent Ratiometric pH Imaging. *RSC Adv.* **2012**, *2*, 968–973.
45. Slowing, I.; Trewyn, B. G.; Lin, V. S. Y. Effect of Surface Functionalization of MCM-41-Type Mesoporous Silica Nanoparticles on the Endocytosis by Human Cancer Cells. *J. Am. Chem. Soc.* **2006**, *128*, 14792–14793.
46. Whiteowen, C.; Alexander, J. W.; Sramkoski, R. M.; Babcock, G. F. Rapid Whole-Blood Microassay Using Flow Cytometry for Measuring Neutrophil Phagocytosis. *J. Clin. Microbiol.* **1992**, *30*, 2071–2076.
47. Song, H. T.; Choi, J. S.; Huh, Y. M.; Kim, S.; Jun, Y. W.; Suh, J. S.; Cheon, J. Surface Modulation of Magnetic Nanocrystals in the Development of Highly Efficient Magnetic Resonance Probes for Intracellular Labeling. *J. Am. Chem. Soc.* **2005**, *127*, 9992–9993.
48. Meng, H.; Yang, S.; Li, Z. X.; Xia, T.; Chen, J.; Ji, Z. X.; Zhang, H. Y.; Wang, X.; Lin, S. J.; Huang, C.; *et al*. Aspect Ratio Determines the Quantity of Mesoporous Silica Nanoparticle

Uptake by a Small Gtpase-Dependent Macropinocytosis Mechanism. *ACS Nano* **2011**, *5*, 4434–4447.
49. Huang, D. M.; Hung, Y.; Ko, B. S.; Hsu, S. C.; Chen, W. H.; Chien, C. L.; Tsai, C. P.; Kuo, C. T.; Kang, J. C.; Yang, C. S.; *et al*. Highly Efficient Cellular Labeling of Mesoporous Nanoparticles in Human Mesenchymal Stem Cells: Implication for Stem Cell Tracking. *FASEB J.* **2005**, *19*, 2014–2016.
50. Kang, B.; Chang, S. Q.; Dai, Y. D.; Yu, D. C.; Chen, D. Cell Response to Carbon Nanotubes: Size-Dependent Intracellular Uptake Mechanism and Subcellular Fate. *Small* **2010**, *6*, 2362–2366.
51. Heuser, J. E.; Anderson, R. G. W. Hypertonic Media Inhibit Receptor-Mediated Endocytosis by Blocking Clathrin-Coated Pit Formation. *J. Cell Biol.* **1989**, *108*, 389–400.
52. Orlandi, P. A.; Fishman, P. H. Filipin-Dependent Inhibition of Cholera Toxin: Evidence for Toxin Internalization and Activation through Caveolae-Like Domains. *J. Cell Biol.* **1998**, *141*, 905–915.
53. Schnitzer, J. E.; Oh, P.; Pinney, E.; Allard, J. Filipin-Sensitive Caveolae-Mediated Transport in Endothelium-Reduced Transcytosis, Scavenger Endocytosis, and Capillary-Permeability of Select Macromolecules. *J. Cell Biol.* **1994**, *127*, 1217–1232.
54. Thomsen, P.; Roepstorff, K.; Stahlhut, M.; van Deurs, B. Caveolae Are Highly Immobile Plasma Membrane Microdomains, Which Are Not Involved in Constitutive Endocytic Trafficking. *Mol. Biol. Cell* **2002**, *13*, 238–250.
55. Torgersen, M. L.; Skretting, G.; van Deurs, B.; Sandvig, K. Internalization of Cholera Toxin by Different Endocytic Mechanisms. *J. Cell Sci.* **2001**, *114*, 3737–3747.
56. Matteoni, R.; Kreis, T. E. Translocation and Clustering of Endosomes and Lysosomes Depends on Microtubules. *J. Cell Biol.* **1987**, *105*, 1253–1265.
57. Vida, T. A.; Emr, S. D. A New Vital Stain for Visualizing Vacuolar Membrane Dynamics and Endocytosis in Yeast. *J. Cell Biol.* **1995**, *128*, 779–792.
58. Slowing, I. I.; Vivero-Escoto, J. L.; Zhao, Y.; Kandel, K.; Peeraphatdit, C.; Trewyn, B. G.; Lin, V. S. Y. Exocytosis of Mesoporous Silica Nanoparticles from Mammalian Cells: From Asymmetric Cell-to-Cell Transfer to Protein Harvesting. *Small* **2011**, *7*, 1526–1532.
59. Yanes, R. E.; Tarn, D.; Hwang, A. A.; Ferris, D. P.; Sherman, S. P.; Thomas, C. R.; Lu, J.; Pyle, A. D.; Zink, J. I.; Tamanoi, F. Involvement of Lysosomal Exocytosis in the Excretion of Mesoporous Silica Nanoparticles and Enhancement of the Drug Delivery Effect by Exocytosis Inhibition. *Small* **2013**, *9*, 697–704.
60. Ono, K.; Wang, X. F.; Han, J. H. Resistance to Tumor Necrosis Factor-Induced Cell Death Mediated by PMCA4 Deficiency. *Mol. Cell. Biol.* **2001**, *21*, 8276–8288.
61. Zimmerberg, J.; Sardet, C.; Epel, D. Exocytosis of Sea-Urchin Egg Cortical Vesicles *in Vitro* Is Retarded by Hyperosmotic Sucrose-Kinetics of Fusion Monitored by Quantitative Light-Scattering Microscopy. *J. Cell Biol.* **1985**, *101*, 2398–2410.
62. Dombu, C. Y.; Kroubi, M.; Zibouche, R.; Matran, R.; Betbeder, D. Characterization of Endocytosis and Exocytosis of Cationic Nanoparticles in Airway Epithelium Cells. *Nanotechnology* **2010**, *21*, 355102.
63. Bindokas, V. P.; Jordan, J.; Lee, C. C.; Miller, R. J. Superoxide Production in Rat Hippocampal Neurons: Selective Imaging with Hydroethidine. *J. Neurosci.* **1996**, *16*, 1324–1336.
64. Rosner, M. H.; Vigano, M. A.; Ozato, K.; Timmons, P. M.; Poirier, F.; Rigby, P. W. J.; Staudt, L. M. A POU-Domain Transcription Factor in Early Stem-Cells and Germ-Cells of the Mammalian Embryo. *Nature* **1990**, *345*, 686–692.
65. Okamoto, K.; Okazawa, H.; Okuda, A.; Sakai, M.; Muramatsu, M.; Hamada, H. A Novel Octamer Binding Transcription Factor Is Differentially Expressed in Mouse Embryonic-Cells. *Cell* **1990**, *60*, 461–472.
66. Burdon, T.; Smith, A.; Savatier, P. Signalling, Cell Cycle and Pluripotency in Embryonic Stem Cells. *Trends Cell Biol.* **2002**, *12*, 432–438.
67. Pesce, M.; Wang, X. Y.; Wolgemuth, D. J.; Scholer, H. Differential Expression of the Oct-4 Transcription Factor during Mouse Germ Cell Differentiation. *Mech. Dev.* **1998**, *71*, 89–98.
68. Fenderson, B. A.; Andrews, P. W.; Nudelman, E.; Clausen, H.; Hakomori, S. I. Glycolipid Core Structure Switching from Globo- to Lacto- and Ganglio-Series During Retinoic Acid-Induced Differentiation of TERA-2-Derived Human Embryonal Carcinoma Cells. *Dev. Biol.* **1987**, *122*, 21–34.
69. Knoepfler, P. S. Deconstructing Stem Cell Tumorigenicity: A Roadmap to Safe Regenerative Medicine. *Stem Cells* **2009**, *27*, 1050–1056.
70. Chiou, S. H.; Jiang, B. H.; Yu, Y. L.; Chou, S. J.; Tsai, P. H.; Chang, W. C.; Chen, L. K.; Chen, L. H.; Chien, Y.; Chiou, G. Y. Poly(ADP-Ribose) Polymerase 1 Regulates Nuclear Reprogramming and Promotes iPSC Generation without c-Myc. *J. Exp. Med.* **2013**, *210*, 85–98.
71. Ying, Q. L.; Wray, J.; Nichols, J.; Batlle-Morera, L.; Doble, B.; Woodgett, J.; Cohen, P.; Smith, A. The Ground State of Embryonic Stem Cell Self-Renewal. *Nature* **2008**, *453*, 519–523.
72. Niwa, H.; Burdon, T.; Chambers, I.; Smith, A. Self-Renewal of Pluripotent Embryonic Stem Cells Is Mediated *via* Activation of STAT3. *Genes Dev.* **1998**, *12*, 2048–2060.
73. Brafman, D. A.; Chang, C. W.; Fernandez, A.; Willert, K.; Varghese, S.; Chien, S. Long-Term Human Pluripotent Stem Cell Self-Renewal on Synthetic Polymer Surfaces. *Biomaterials* **2010**, *31*, 9135–9144.
74. Li, B.; Ma, Y. X.; Wang, S.; Moran, P. M. Influence of Carboxyl Group Density on Neuron Cell Attachment and Differentiation Behavior: Gradient-Guided Neurite Outgrowth. *Biomaterials* **2005**, *26*, 4956–4963.
75. Ruponen, M.; Ylä-Herttuala, S.; Urtti, A. Interactions of Polymeric and Liposomal Gene Delivery Systems with Extracellular Glycosaminoglycans: Physicochemical and Transfection Studies. *Biochim. Biophys. Acta* **1999**, *1415*, 331–341.
76. Ziraksaz, Z.; Nomani, A.; Soleimani, M.; Bakhshandeh, B.; Arefian, E.; Haririan, I.; Tabbakhian, M. Evaluation of Cationic Dendrimer and Lipid As Transfection Reagents of Short RNAs for Stem Cell Modification. *Int. J. Pharm.* **2013**, *448*, 231–238.
77. Yang, Z.; Sahay, G.; Sriadibhatla, S.; Kabanov, A. V. Amphiphilic Block Copolymers Enhance Cellular Uptake and Nuclear Entry of Polyplex-Delivered DNA. *Bioconjugate Chem.* **2008**, *19*, 1987–1994.
78. Nishikawa, T.; Iwakiri, N.; Kaneko, Y.; Taguchi, A.; Fukushima, K.; Mori, H.; Morone, N.; Kadokawa, J.-i. Nitric Oxide Release in Human Aortic Endothelial Cells Mediated by Delivery of Amphiphilic Polysiloxane Nanoparticles to Caveolae. *Biomacromolecules* **2009**, *10*, 2074–2085.
79. Sorkin, A.; von Zastrow, M. Signal Transduction and Endocytosis: Close Encounters of Many Kinds. *Nat. Rev. Mol. Cell Biol.* **2002**, *3*, 600–614.
80. Miaczynska, M.; Pelkmans, L.; Zerial, M. Not Just a Sink: Endosomes in Control of Signal Transduction. *Curr. Opin. Cell Biol.* **2004**, *16*, 400–406.
81. Schenck, A.; Goto-Silva, L.; Collinet, C.; Rhinn, M.; Giner, A.; Habermann, B.; Brand, M.; Zerial, M. The Endosomal Protein Appl1Mediates Akt Substrate Specificity and Cell Survival in Vertebrate Development. *Cell* **2008**, *133*, 486–497.
82. Cereghini, S. Liver-Enriched Transcription Factors and Hepatocyte Differentiation. *FASEB J.* **1996**, *10*, 267–282.
83. Lee, C. S.; Friedman, J. R.; Fulmer, J. T.; Kaestner, K. H. The Initiation of Liver Development Is Dependent on Foxa Transcription Factors. *Nature* **2005**, *435*, 944–947.
84. Duncan, S. A.; Nagy, A.; Chan, W. Murine Gastrulation Requires HNF-4 Regulated Gene Expression in the Visceral Endoderm: Tetraploid Rescue of HNF-4(−/−) Embryos. *Development* **1997**, *124*, 279–287.
85. Perlmutter, D. H. Autophagic Disposal of the Aggregation-Prone Protein That Causes Liver Inflammation and Carcinogenesis in α-1-Antitrypsin Deficiency. *Cell Death Differ.* **2009**, *16*, 39–45.

86. Ko, K. S.; Tomasi, M. L.; Iglesias-Ara, A.; French, B. A.; French, S. W.; Romani, K.; Jose Lozano, J.; Oh, P.; He, L.; Stiles, B. L.; *et al*. Liver-Specific Deletion of Prohibitin 1 Results in Spontaneous Liver Injury, Fibrosis, and Hepatocellular Carcinoma in Mice. *Hepatology* **2010**, *52*, 2096–2108.
87. Sommer, C. A.; Stadtfeld, M.; Murphy, G. J.; Hochedlinger, K.; Kotton, D. N.; Mostoslavsky, G. Induced Pluripotent Stem Cell Generation Using a Single Lentiviral Stem Cell Cassette. *Stem Cells* **2009**, *27*, 543–549.